AD-A185 100 NUMERICAL PREDICTION OF UNSTEADY SHEET CAVITATION ON MARINE PROPELLERS(U) DEFENCE RESEARCH ESTABLISHMENT ATLANTIC DARTMOUTH (NOVA SCOTIA) D J NOBLE JUL 87 1/1

UNCLASSIFIED DREA-TM-87/203 F/G 20/4 NL

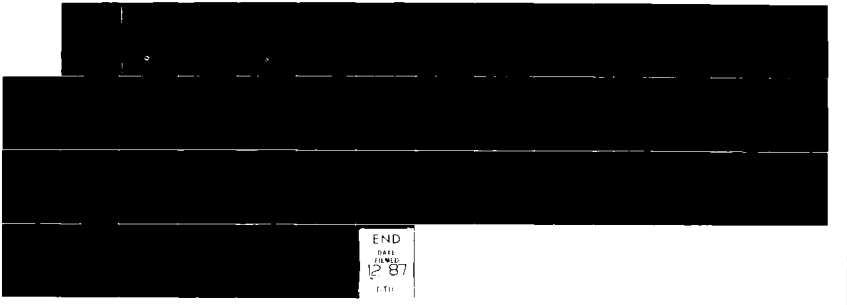

END
DATE FILMED
12 87
DTIC

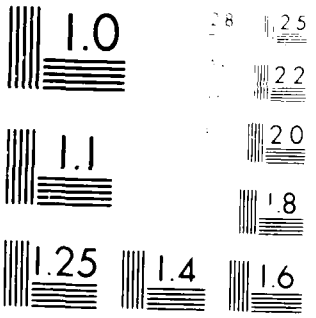
1.0
1.1
1.25
1.4
1.6
1.8
2.0
2.2
2.5

UNLIMITED DISTRIBUTION

National Defence
Research and Development Branch

Défense nationale
Bureau de recherche et développement

TECHNICAL MEMORANDUM 87/203
July 1987

NUMERICAL PREDICTION OF UNSTEADY SHEET CAVITATION ON MARINE PROPELLERS

D.J. Noble

Defence Research Establishment Atlantic

Centre de Recherches pour la Défense Atlantique

Canada

DEFENCE RESEARCH ESTABLISHMENT ATLANTIC

9 GROVE STREET
P O BOX 1012
DARTMOUTH, N S
B2Y 3Z7

TELEPHONE
(902) 426-3100

CENTRE DE RECHERCHES POUR LA DÉFENSE ATLANTIQUE

9 GROVE STREET
C P 1012
DARTMOUTH, N E
B2Y 3Z7

UNLIMITED DISTRIBUTION

National Defence
Research and Development Branch

Défense nationale
Bureau de recherche et développement

NUMERICAL PREDICTION OF UNSTEADY SHEET CAVITATION ON MARINE PROPELLERS

D.J. Noble

July 1987

Approved by B.F. Peters A/Director/Technology Division

DISTRIBUTION APPROVED BY

A/D/TD

TECHNICAL MEMORANDUM 87/203

Defence Research Establishment Atlantic

Centre de Recherches pour la Défense Atlantique

Canada

Abstract

This document describes the theory and numerical methods used in the propeller analysis program CAVITY that has been developed at the Defence Research Establishment Atlantic (DREA) for the prediction of periodic back sheet cavitation on marine propellers operating in a ship's wake. Sheet cavitation chordwise extents and thickness distributions can be predicted at up to 60 blade angular positions per revolution for a given propeller geometry, operating condition and ship wake inflow in the propeller rotation plane. The procedures used in CAVITY are based on lifting surface methods developed at the Massachusetts Institute of Technology (MIT) as an extension of the PUF-2 code for predicting both steady and unsteady propulsive performance characteristics of marine propellers. The original MIT procedures for the prediction of back sheet cavitation are reviewed and some modifications concerning chordwise distributions of singularities and propeller wake modelling are described. These changes are incorporated to improve predictions of leading edge cavitation development as well as results obtained at off-design operating conditions. Numerical extents obtained with CAVITY are compared to available experimental data. Provided that representative ship wake data are used, the predictions to date for back sheet cavitation show good agreement with experimentally observed extents developing on thin blade sections.

Résumé

Le présent document décrit la théorie et les méthodes numériques utilisées dans le programme d'analyse des hélices CAVITY mis au point au Centre de recherches pour la défense de l'Atlantique (CRDA) pour la prévision de la rétrocavitation laminaire périodique engendrée par les hélices marines travaillant dans le sillage d'un navire. L'ampleur et les distributions d'épaisseur de la cavitation laminaire dans le sens axial peuvent être prédites pour jusqu'à 60 positions angulaires par révolution des pales pour une géométrie de l'hélice, des conditions de fonctionnement et un écoulement attribuable au sillage du navire dans le plan de rotation de l'hélice donnés. Les traitements utilisés par le programme CAVITY sont basés sur les méthodes de la surface portante élaborées au Massachusetts Instititute of Technology (MIT) à titre d'extension du code PUF-2 pour la prévision des caractéristiques du rendement en propulsion des hélices marines en régimes permanent et non permanent. Les traitements d'origine du MIT pour la prévision de la rétrocavitation laminaire sont examinés et on décrit certaines modifications concernant les distributions des points singuliers dans le sens axial ainsi que la modélisation du sillage de l'hélice. Ces modifications sont incorporées afin d'améliorer les prévisions de l'apparition de la cavitation au bord d'attaque et les résultats obtenus dans des conditions non nominales de fonctionnement. Les plages de valeurs numériques obtenues au moyen de CAVITY sont comparées aux données expérimentales disponibles. Pourvu qu'on utilise des données représentatives pour le sillage du navire, on a obtenu jusqu'à maintenant des prévisions de la rétrocavitation laminaire qui concordent bien avec ce qui est observé lors des expériences sur des profils minces de pales.

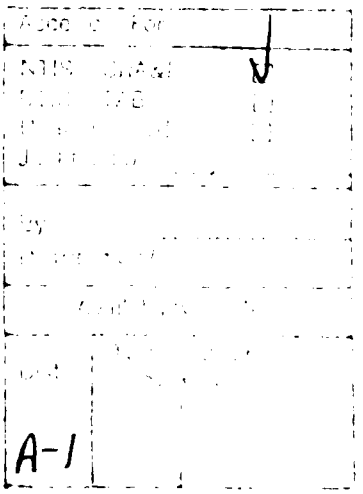

Contents

1 Introduction

This document describes the results of the first phase in the development of a series of computer programs for analyzing the effects of unsteady cavitation in the flow around marine propellers. This initial phase involves the prediction of periodic sheet cavitation chordwise extents and thickness distributions on the back or upstream side of propeller blades operating in a ship's wake. The resulting program, named CAVITY, includes various features of recently published methods in an effort to obtain good correlation with experimental data.

In future phases, it is intended to develop additional computer codes to calculate far field noise and the pressure induced on the ship hull associated with back sheet cavitation. The radiated noise and hull pressure predictions require consideration of the effects of the free water surface and a hull boundary in the vicinity of the propeller. On completion of these codes, it would be useful to extend the cavitation, noise and hull pressure analysis to include other types of propeller cavitation. This could involve sheet cavitation development on the face or downstream surface of the blades as well as cavitation forming in the propeller tip vortices in combination with the back sheet results.

The development of unsteady cavitation on and around marine propellers is encouraged by ship design trends towards greater power and operating speeds. The increased nonuniformity of the wake deficit region behind ships with V-shaped aft ends, reduced propeller tip immersion depths in restricted drafts, and increased propeller rotation speeds are all conditions favourable to pulsating cavitation. Taken together, these conditions increase the likelihood that the pressure in the flow around the propeller will decrease below the vapour pressure of water and promote the rapid growth and collapse of cavitation over portions of a blade's revolution.

The undesirable consequences of unsteady cavitation provide a strong motivation for both analytical and experimental research in this area of hydrodynamics. Rapid fluctuations in propeller cavitation have been observed experimentally to correspond to significant increases in the vibration of nearby struts, rudders, and hull panels as well as in radiated noise levels. If allowed to develop at increased speeds, pulsating cavitation can cause sudden thrust losses and, over extended periods of time, can lead to blade erosion. In the propeller designer's attempts to alleviate these undesirable effects, an accurate and reliable analytical prediction method would be a very useful tool; however, the state of the art of propeller cavitation prediction methods is still a long way from accurately describing all aspects of this complex problem in two-phase flow.

There are a number of physical conditions known to affect the inception, growth, and collapse of propeller cavitation. Most of the key aspects are described by Kuiper[1] in a report produced for the Netherlands Ship Model Basin Cooperative Research Ships program. Cavitation development can be affected by the diffusion of gas or vapour into or out of the cavity,

surface tension, blade surface roughness, and boundary layer effects, as well as the variable flow into the propeller. Inflow variations can be generated by upstream hull and appendage wakes, ship maneuvers and ship motions in a seaway. Developing adequate theoretical models for many of these complex physical interactions is a formidable task. The approach taken in the numerical methods described here is an attempt to obtain a good estimate of periodic sheet cavitation development with a simple model that can be readily coupled with existing lifting surface procedures.

This type of model has been used by Lee[2] as a extension of the procedures in the lifting surface analysis code PUF-2 developed at MIT by Kerwin and Lee[3] for the prediction of net unsteady forces and moments on marine propellers. In Lee's method, singularity distributions are used on the blade mean camber surfaces and downstream wake sheets. Vortices are used to provide flow circulation both around the blades and in their wakes, and sources are used to represent both blade and cavity thickness effects. The vorticity and source distributions induce a potential flow that is used to simulate the flow disturbance created by a cavitating propeller. By appropriately discretizing these singularity distributions, a system of linear equations is established for the strengths of straight line vortex and source segments so as to satisfy prescribed boundary conditions and conservation laws. The method provides unsteady, incompressible, potential flow solutions directly in the time domain and was selected as the basis for the DREA program CAVITY because of the ease of its adaption to complex propeller geometries, and for its ability to handle three dimensional spanwise interactions and fairly rapid cavity time variations. It is also an extension of the PUF-2 code which has correlated well with experimental data for propeller performance characteristics.

Before describing the numerical procedures used in CAVITY, the common basic assumptions and governing equations of Lee's original method are reviewed in Section 2 to establish the limitations of the theory. Section 3 then describes the singularity discretization emphasizing some differences compared with the earlier methods of Kerwin and Lee. A resulting system of linear equations is established in Section 4 together with a solution procedure that includes initial conditions and techniques for time stepping and updating singularity strengths. The resulting program is then verified in Section 5 by comparing sheet cavitation predictions with experimental data.

2 Assumptions and Governing Equations

To give some background for the procedures used in program CAVITY, the basic assumptions of Lee's original method are reviewed here. First, the blades are assumed to be thin, rigid, equally-spaced, and identical surfaces of arbitrary shape. All sections of the blade operate at small angle of attack. The assumption of small angles of attack usually implies that in a real fluid the viscous effects can be confined to thin, attached boundary layers on the blade surfaces and to thin, downstream wake sheets outside which inviscid, potential flow solutions are valid.

As in the PUF-2 code, a pitch angle reduction can be applied to blade sections to approximate the effects of boundary layer thickness and flow separation near the trailing edge. Extraneous boundaries such as a propeller hub or the ship hull and appendages are neglected except that the upstream hull boundary layer and appendage wake effects are included in the specified inflow velocity distribution into the plane of propeller rotation. This nonuniform inflow consists of the uniform onset flow due to a constant forward ship speed and three spatially varying velocity components of the ship wake that are assumed to be independent of time and to have negligible variation over the propeller axial extent relative to a ship fixed reference frame.

The net effect of the ship wake inflow can be described in terms of the Taylor wake fraction, $w_T = 1 - (V_A/V_s)$, hereafter simply referred to as the wake fraction, where V_A is the volumetric average of the axial component of the ship wake inflow velocity distributed over the propeller disc, and V_s is the ship speed. The nominal wake fraction can be obtained from direct measurements of the axial inflow distribution over the propeller rotation plane of a towed ship model, without propellers fitted. An effective wake fraction based on thrust coefficient identity can be obtained through analysis of either model or full scale ship propulsion tests as $w_{T_T} = 1 - (J_{O_T}/J_P)$, where $J_P = V_s/(nD)$ is the apparent advance coefficient for a propeller of diameter D operating at n revolutions per second in the wake of a model or full scale ship moving at speed V_s, and J_{O_T} is the propeller open water test advance coefficient that generates the same thrust coefficient as obtained in the behind condition. An effective wake fraction, $w_{T_Q} = 1 - (J_{O_Q}/J_P)$, can also be defined based on torque coefficient identity. When the propeller operates in the behind condition at any vessel speed and shaft revolution rate, a given estimate of the wake fraction can be used to define the operating advance coefficient as $J = V_A/(nD)$, using $V_A = V_s(1 - w_T)$ for the volumetric mean axial inflow velocity.

Since lifting surface methods require estimates of the ship wake inflow velocity distributed over the blade surfaces, the reliability of the cavitation prediction method depends on the accuracy of this distribution. Much effort is currently being directed towards the development of correction procedures to be applied to the axial component of the distributed nominal wake velocity. Procedures are currently available which attempt to correct these nominal wake data for hull boundary layer differences between model and full scale ships[4] and also for propeller-generated, inviscid, rotational flow effects on the incoming wake vorticity distribution[5,6]. These modifications to the nominal axial wake distribution are referred to as Reynolds number scaling and propeller-wake interaction effects respectively. Application of these procedures results in an estimate of the full scale, effective wake distribution over the propeller rotation plane. The effective wake distributions obtained with these methods are approximations to the difference between the axial component of the total velocity distribution that would be present with propellers operating, and the axial component of the distribution of propeller-induced, potential flow velocity as generated by lifting surface singularities. These effective wake distributions can also be volumetrically averaged over the propeller plane to provide numerical estimates of the effective wake fraction.

Reynolds number scaling and effective wake modifications to the nominal wake distribution are most important for single screw vessels for which the major portion of each blade encounters a large wake deficit region near the centre plane of the ship. For twin propeller configurations of interest at DREA, for which the blade tips pass through only the outer extremities of the wake

deficit region, the nominal wake data should provide an adequate representation of the effective model and full scale wake distributions; however, the wake velocity measurements should use a sufficiently fine grid of data points to adequately resolve the higher harmonics of the wake angular coordinate in the plane of rotation.

As far as the sheet cavitation itself is concerned, Lee's method assumes that cavities are thin, continuous volumes developing on the back surface, starting from the blade leading edge and remaining attached to the blade as it rotates. Diffusion of gas or vapour into or out of the cavity, surface tension, blade surface roughness and leading edge flow separation effects are not treated. The cavity is also maintained at a constant pressure equal to the vapour pressure of water from inception to collapse.

As a direct result of these assumptions and constraints, the predicted sheet cavitation is periodic in time at the shaft rate and is repeated identically on each blade every revolution. Shaft rate periodic cavitation repeated on equally-spaced, identical blades generates field pressures that are periodic at the blade passing frequency. In practice, unsteady sheet cavitation can generate frequency spectra with both broadband components and narrowband lines that are not necessarily at multiples of the shaft rate due to the neglected effects of random turbulence and deterministic time variations in the inflow. These effects combined with inter-blade differences in geometry and surface condition and the presence of other types of random or generally time varying cavitation both attached to and separating from the blades are responsible for generating acoustic pressures and propeller induced hull pressures that are not necessarily periodic at the blade rate. Vibrating surfaces and other sources of noise in the flow or within the ship may also be prevalent in the acoustic spectra. Experimental evidence to date does reveal dominant shaft and blade rate harmonics usually in the low frequency end of the spectra and it is the low frequency, macroscopic development of sheet cavitation that Lee's theory is predicting.

It now remains to define the governing equations and boundary conditions to be satisfied by the propeller induced flow in a blade fixed reference frame. In this rotating frame, the velocity induced at points in the fluid moving with the blade, which are outside the singularity regions of the vortex and source distributions, is a solution of the equation of mass conservation for an incompressible flow which takes the form of the vanishing of the divergence of the induced velocity vector $\vec{V}$.

$$\vec{\nabla} \cdot \vec{V} = 0 \tag{2.1}$$

Here, $\vec{\nabla}$ denotes the vector gradient operator. With the assumption that the propeller induced flow is irrotational in the blade fixed reference frame, the induced velocity vector can be written as the gradient of a scalar potential function Φ, and equation (2.1) is equivalent to the vanishing of the Laplacian of the induced velocity potential.

$$\nabla^2 \Phi = 0 \tag{2.2}$$

The free field solutions to these equations, as produced by source and vortex distributions, are required to satisfy a quiescence condition that induced flow velocities vanish far upstream of

the propeller.

In the lifting surface procedures developed by Kerwin and Lee, continuous singularity distributions over the mean camber surfaces of the blades and their downstream wake sheets are discretized to form a mesh of straight line source and vortex segments. The source strength distributions for blade and sheet cavity thickness represent jump discontinuities in normal velocity across the blade mean surfaces, while distributed vorticity is used to represent a tangential velocity jump. Blade thickness distributions are known and constant in time and the associated source strengths are obtained by application of thin airfoil theory to each fixed radius section of a blade. Cavity thickness source strengths are time dependent and, as with cavity chordwise extents and the vortex strengths, are determined from Lee's time stepping solution procedure. The vortex strengths are vectors lying on the mean surfaces and wake sheets, and can be resolved into components in two directions. Spanwise loading variations on three dimensional lifting surfaces generate streamwise directed free trailing vortices while time variations of loading cause spanwise vortices to be shed into the downstream wake. It is convenient to use a mesh of spanwise and streamwise directed vortex segments, bound and trailing segments on the blade mean surfaces and shed and trailing segments on the downstream wake sheet. The details of the locations of singularity segments used in program CAVITY are given in Section 3. As shown by Kerwin and Lee[3], vortex conservation laws and Kelvin's theorems for circulation conservation can be used to define all vortex segment strengths in terms of the spanwise directed bound vortex segment strengths distributed on the blade mean surfaces.

In this discretized model, each singularity segment is assigned a unique strength constant over its length but allowed to vary in time as the blades rotate. For a single source segment of strength Q along a straight line from point P_1 to point P_2, the induced potential Φ^Q at any time t and any field location $\vec{r}$ moving with the blades can be expressed as:

$$\Phi^Q(\vec{r},t) = Q(t)\phi^Q(\vec{r}) \tag{2.3}$$

$$\phi^Q(\vec{r}) = -\frac{1}{4\pi}\int_{P_1}^{P_2}\frac{dl}{R} \tag{2.4}$$

Here, ϕ^Q represents the potential at $\vec{r}$ from a unit strength line source segment and R is the distance from an infinitesimal element of length dl on the line source to the field point. Taking the gradient of equation (2.3), the induced velocity $\vec{V}^Q$ at $\vec{r}$ from this line source segment becomes:

$$\vec{V}^Q(\vec{r},t) = Q(t)\vec{v}^Q(\vec{r}) \tag{2.5}$$

$$\vec{v}^Q(\vec{r}) = -\frac{1}{4\pi}\int_{P_1}^{P_2}\vec{\nabla}\left(\frac{1}{R}\right)dl \tag{2.6}$$

The velocity $\vec{v}^Q$ is induced at $\vec{r}$ by a unit strength line source segment from P_1 to P_2.

From the law of Biot and Savart, the velocity induced at field point $\vec{r}$ from a single vortex segment of strength Γ along a straight line from P_1 to P_2 takes the form:

$$\vec{V}^{\Gamma}(\vec{r},t) = \Gamma(t)\vec{v}^{\Gamma}(\vec{r}) \tag{2.7}$$

$$\vec{v}^{\Gamma}(\vec{r}) = \frac{1}{4\pi}\int_{P_1}^{P_2} \frac{d\vec{l} \times \vec{R}}{R^3} \tag{2.8}$$

Here, $\vec{R}$ is the relative position vector of magnitude R, the distance to the field point from an infinitesimal vector element of the line vortex $d\vec{l}$ of magnitude dl. Equations (2.6) and (2.8) can be integrated over the length of an arbitrarily located segment to yield simple expressions for the unit strength contributions in terms of blade fixed, propeller centred Cartesian coordinates of P_1, P_2 and a field location $\vec{r}$ moving with the blades. These formulas, taken from Kerwin and Lee[3], are summarized in Appendix A.

Because equations (2.1) and (2.2) are linear in velocity and potential, the principle of linear superposition applies and the total velocity or potential induced by a mesh of discrete line source and vortex segments distributed over blade mean camber surfaces and downstream wake sheets is obtained by summing up contributions from the individual segments. The formulas for induced velocity and potential are used to enforce boundary conditions at selected control points on a designated key blade so as to yield a system of linear equations for the unknown strengths of bound vortex and cavity source segments at each instant of time. As the key blade rotates, the time varying singularity strengths on the other blades and their wakes are updated so that their influence on the solution for the key blade is included after a few revolutions of time stepping. Details of the control point locations at which the boundary conditions are enforced are found in Section 3.

One of the main boundary requirements to be satisfied is the flow tangency condition of zero net flow normal to the impermeable, rigid surfaces of the blades. In the lifting surface approximation for thin blades, this condition is applied at control points on the mean camber surface and is expressed in the form:

$$\vec{n} \cdot \vec{V}_T = 0 \tag{2.9}$$

$$\vec{V}_T = \vec{V}_\infty + \vec{V}_I \tag{2.10}$$

Here, $\vec{n}$ is the unit vector normal to the camber surface at each control point and $\vec{V}_T$ is the total velocity at the control point. This total velocity is composed of $\vec{V}_\infty$, the known relative inflow velocity (i.e. the mean flow components opposite to both the blade rotational velocity and uniform forward ship speed as well as the ship wake inflow variations), and also $\vec{V}_I$, the total velocity induced by singularity segments distributed over the blade mean camber surfaces and downstream wake sheets. A continuous tangential flow is obtained at the blade trailing edges by ensuring that the Kutta condition is satisfied there.

For cavitating regions of the flow about the blades, the dynamic condition applied at the cavity/water interface moving with the flow is to prescribe the pressure at the interface as the vapour pressure of water at each instant of time as the cavity grows and collapses. In order to enforce this constant vapour pressure over the entire cavity extent in terms of the local induced velocities from the singularities, the flow adjacent to the cavity surface must satisfy the unsteady Bernoulli equation written relative to blade fixed coordinates[7]. For this purpose, it is convenient to write the Bernoulli equation in an orthogonal coordinate system (ξ, η, ς) fixed on the mean camber surface of the blade. The ξ coordinate is tangent to the camber surface in a downstream chordwise sense at fixed radius, the η coordinate is tangent to the mean surface and perpendicular to the ξ coordinate in an outward spanwise sense, and the ς coordinate is directed outwards normal to the camber surface.

Considering flow velocity components along these coordinate directions, the total velocity includes a steady relative inflow that is aligned essentially in the ξ direction at each radius r, and has a magnitude U defined as:

$$U = \sqrt{V_a^2 + (r\omega)^2} \tag{2.11}$$

Here, V_a is the axial component of the circumferential mean inflow which is expressed as a function of r, and ω is the angular velocity of the propeller. In addition, perturbative velocity components u, v and w are defined in the ξ, η and ς coordinate directions respectively. These perturbative components are singularity induced velocities. Relative to (ξ, η, ς) coordinates rotating with the blade and advancing axially with velocity V_a at each fixed radius, the unsteady Bernoulli equation, evaluated both at a local cavity control point and at a reference point at the depth of the shaft centre at upstream infinity, takes the form:

$$p + \frac{1}{2}\rho(V_T^2 - U^2) + \rho\frac{\partial \Phi}{\partial t} + \rho g y_o = p_\infty \tag{2.12}$$

Here the total velocity V_T at the control point is obtained from the the following relation:

$$V_T^2 = (U + u)^2 + v^2 + w^2 \tag{2.13}$$

The pressure p_∞, at shaft depth H, far upstream of the propeller is given by:

$$p_\infty = p_{atm} + \rho g H \tag{2.14}$$

In the preceding equations, p_{atm} is the atmospheric pressure at the water surface, ρ is water density, g is the acceleration due to gravity, p and $\frac{\partial \Phi}{\partial t}$ are the local pressure and potential time derivative at the control point, and y_o is the periodic vertical coordinate of the control point relative to the shaft centre. A version of equation (2.12) which is linear in perturbation velocity is obtained by neglecting products of small quantities in equation (2.13) (i.e. by using $V_T^2 \simeq U^2 + 2Uu$) to give:

$$p - p_\infty = -(\rho \frac{\partial \Phi}{\partial t} + \rho U u + \rho g y_o) \tag{2.15}$$

This dynamic condition for the sheet cavity is enforced by starting with the fully wetted blade solution, creating a small initial sheet cavity extent on each chordwise strip of the blade and suitably adjusting this extent until the pressure p according to equation (2.15) equals the vapour pressure of water at all control points defined within the cavity extent. If the extent tends to zero before this pressure can be reduced to the vapour pressure, then that chordwise section of the blade is considered fully wetted or non-cavitating. Further details of the iterative procedures used to enforce this condition are provided in Section 4.

The cavity source strengths and associated thicknesses normal to the camber surface are further restrained by the application of a cavity closure condition. In Lee's method, this condition enforces the vanishing of cavity thickness at the leading and trailing ends of the cavity chordwise extent. If $h(\xi, t)$ is the instantaneous cavity thickness normal to the camber surface as a function of the ξ coordinate, starting at the cavity leading end on each fixed radius section, then:

$$h(0, t) = h(L, t) = 0 \tag{2.16}$$

Here, L is the cavity chordwise extent in the ξ coordinate direction. To relate source strength and cavity thickness, Lee defines the following linear relationship between source segment strength, Q, and cavity thickness, h.

$$Q = \Delta\xi \cos\epsilon (\frac{\partial h}{\partial t} + U \frac{\partial h}{\partial \xi}) \tag{2.17}$$

The interval $\Delta\xi$ is the element of chordwise extent that a concentrated, spanwise directed line source segment represents, and ϵ is the angle this line source is oriented relative to the η coordinate direction. To summarize Lee's method of satisfying cavity closure, Appendix B contains a discretized version of equation (2.17) using finite differences in t and ξ, a resulting recurrence formula for instantaneous cavity thickness and a cavity closure relation satisfied by cavity source segment strengths within the cavity extent.

3 Singularity Discretization

This section describes the positioning of the end points of vortex and source line segments on the blade mean surfaces and downstream wake sheets, together with the locations of control points at which the boundary conditions for flow tangency and cavity pressure are enforced.

Differences between the singularity and control point locations used in program CAVITY and Lee's original method are noted.

Figures 1a and 1b illustrate the grid of vortex line segments used on the blade mean surface and near wake sheet, as well as the vortex modelling used for a rolled up ultimate wake. Currently ninety spanwise directed bound vortex segments are used on the blade. Nine spanwise segments are positioned from root to tip with end points lying along each of ten lines of fixed percentage chord. Chordwise directed trailing vortex segments then join the bound vortex and first shed wake vortex segment end points along ten lines of fixed radius. The blade trailing vortices extend out into the downstream wake sheet as ten free trailing vortex lines. Fifteen trailing segments are used in the near transition wake extending from the first shed vortex segment endpoints near the blade trailing edge to the location where the wake sheet rolls up. The outer half of the trailing vortex lines converge to form a concentrated tip vortex helix at a separate outer roll up point for each blade while the inner half converge to a single hub vortex line on the extension of the shaft axis downstream of the propeller hub. Shed vortex segments oriented approximately in the radial direction join the end points of the wake trailing vortex segments in the near transition wake and are used to account for instantaneous circulation shed downstream by the time varying loads on blade sections.

This wake roll up model is used in the original PUF-2 code developed by Kerwin and Lee[3]. The near wake geometry is controlled by three parameters: the roll up radius of tip vortices; the increment of angle in the rotation plane that the outermost trailing vortices turn from trailing edge to roll up; and, their pitch angle measured normal to the rotation plane. In the PUF-2 code, provision is made to allow the rolled up tip vortex to further contract radially to an ultimate wake point at a specified rotation angle increment from the trailing edge using the near wake pitch angle. The ultimate wake would then continue downstream as a constant radius helix which could be assigned a different pitch than used in the transition wake. Since the results obtained with PUF-2 are insensitive to small variations of the radius and pitch of this ultimate wake, program CAVITY now uses a fixed radius tip vortex helix downstream of roll up maintaining the near wake pitch angle with respect to the rotation plane.

In Lee's original method for sheet cavitation prediction, there was no roll up of the downstream wake sheets and the free trailing vortices in the wake remained at the radii of the blade trailing vortices and followed helical paths of specified pitch so as to retain the linearity of the problem and better correlate with other solutions obtained from linear theory. The roll up model is used in CAVITY to extend the reliability of the results obtained to a wider range of propeller operating conditions. Assuming that appropriate values of the near wake geometry parameters can be specified, the roll up model improves correlation with experiment for more heavily loaded and off design operating conditions.

In the Kerwin and Lee procedures[2,3], relations are given for propeller centred Cartesian coordinates of points on the blade mean surface in terms of the usual propeller geometric parameters of pitch, rake, skew, chord and camber distributions as well as the local section radius and chord fraction. The same definitions of the geometric variables are used in program CAVITY. Figure 2a illustrates the definitions of back and face surfaces, chord, mean camber surface, thickness and camber offset for a single blade section at any fixed radius while Figure 2b shows the section as it appears on the actual blade and illustrates the definitions of pitch,

rake and skew of the section with the blade in its vertical reference position relative to a ship fixed Cartesian coordinate system at the hub centre.

In the PUF-2 code, bound vortex segment end points are spaced uniformly over the blade radius and are placed at the quarter chord points of equal intervals along fixed radius chordlines. Although retaining the uniform radial spacing used in PUF-2, CAVITY uses a nonuniform chord spacing suggested by Van Houten[8] in his study of cavitation development on large aspect ratio hydrofoils. Lee used a similar chordwise distribution but had segments on the blade shifted towards the trailing edge by one quarter of the bound vortex intervals. The leading edge concentration of Van Houten's chord spacing is beneficial to sheet cavitation development from the blade leading edges.

The radial locations, r^Γ, for the end points of a total of M spanwise directed bound vortex segments, at fixed percentage chord between the hub and tip on the blade mean surface, are obtained from the equations:

$$r^\Gamma_m = r_H + \frac{4m-3}{4}\Delta r\,, \quad m = 1, 2, ..., M+1 \tag{3.1}$$

$$\Delta r = \frac{4(r_T - r_H)}{4M+2} \tag{3.2}$$

Here, r_H is the propeller hub radius and r_T is the tip radius. These trailing vortex segment radii are uniformly spaced Δr apart and range from $\frac{1}{4}\Delta r$ greater than the hub radius to $\frac{1}{4}\Delta r$ less than the tip radius.

In CAVITY, the chord fractions s^Γ of a total of N bound vortex segment end points along any fixed radius arc on the blade mean surface are defined as:

$$s^\Gamma_n = 1 - \cos[\frac{(n-1)\pi}{2N}]\,, \quad n = 1, 2, ..., N \tag{3.3}$$

Note that the first bound vortex segment of each chordwise strip has end points located right at the leading edge, $s = 0$. The bound vortex segments are spaced closer together near the leading edge with the chordwise separation gradually increasing to a maximum at the trailing edge. By continuing this large trailing edge spacing uniformly out into the downstream wake for the shed vortex segments, the Kutta condition of smooth tangential flow at the blade trailing edges is satisfied implicitly.

The equations used in CAVITY to obtain coordinates of the end points of trailing and shed vortex segments in the near transition wake, up to the roll up points, are also defined by Kerwin and Lee[3]. Downstream of roll up, the ultimate wake helix is replaced by a sequence of straight line segments of equal length covering about five revolutions of the helix at the roll up radius and pitch of the near wake.

Figure 3 depicts the relative placement of source and vortex line segments used for a typical m^{th} chordwise strip between any two radius stations r^Γ_m and r^Γ_{m+1} on the blade mean surface and extending into the near wake downstream of the trailing edge. As in the PUF-2

code, the blade thickness source segments are coincident with the bound vortex segments. The cavity thickness source segments, as with those for blade thickness, run in a spanwise sense at fixed percentage chord. The nonuniform chordwise spacing of cavity sources used in program CAVITY is also borrowed from Van Houten[8]. On the blade mean surface, a maximum of N cavity source chord fractions s^Q are defined by the equation:

$$s_n^Q = 1 - \cos[\frac{(n-\frac{1}{2})\pi}{2N}], \quad n = 1, 2, ..., N \tag{3.4}$$

These cavity sources are also concentrated towards the leading edge and are roughly located midway between successive bound vortex segments in each strip. If the sheet cavitation extends beyond the trailing edge in any chordwise strip, additional cavity source segments are placed midway between successive shed vortex segments in the near wake. Lee places his cavity sources exactly midway between bound and shed vortex segments except for the last source on the blade surface which is midway between the last bound vortex and the blade trailing edge. With segments shifted further downstream from the leading edge from those defined by equation (3.4), Lee found it necessary to interchange the locations of the first cavity source segment and cavity pressure control point in each chordwise strip in order to simulate the proper source strength behaviour at the leading edge. However Van Houten found that by having the first bound vortex right at the leading edge, the first cavity source and bound vortex segment strengths can be related using a quarter root singularity behaviour appropriate to the leading edge. The chordwise distributed source and vortex strengths near the leading edge are inversely proportional to the fourth root of the chordwise distance from the leading edge and the strengths of the first cavity line source segment Q_1 and first bound vortex segment Γ_1 can be related by:

$$\frac{Q_1}{\Gamma_1} = \frac{\int_0^{s_2^\Gamma} s^{-1/4}\, ds}{\int_0^{s_1^Q} s^{-1/4}\, ds} = 4^{3/4} \tag{3.5}$$

Here the line segment strength Q_1 is the concentrated representation of the chordwise distributed source strength over the interval $0 \leq s \leq s_2^\Gamma$ and Γ_1 is the concentrated line segment strength of the bound vortex representing distributed vorticity over $0 \leq s \leq s_1^Q$. The chord fractions s_2^Γ and s_1^Q used in equation (3.5) are obtained as approximations to equations (3.3) and (3.4) for small cosine arguments.

Not knowing in advance the sheet cavity extents in each chordwise strip, program CAVITY uses a maximum of fifteen cavity source segments in each of nine strips with all source strengths initially set to zero corresponding to a cavitation free blade. As extents are determined as part of the iterative solution procedures described in Section 4, only the source segments falling within the extent in each strip are turned on and assigned strengths obtained by solving the governing equations.

Figure 3 also shows the locations of control points in a typical chordwise strip. The circular symbols located at the midpoints of cavity source segments that fall on the blade are points at which the flow tangency condition of zero total velocity normal to the mean surface is satisfied.

The X symbols at the midpoints of bound and shed vortex segments are the control points at which cavity pressure is made equal to the vapour pressure of water as the cavity extent grows and collapses. The number of cavity pressure control points used in each chordwise strip at a given blade position then equals the number that fall within the latest estimate of cavity chordwise extent in that strip.

The singularity grid described previously is used for a designated key blade, the only blade on which control points are located and boundary conditions are enforced. Since the distances are relatively large between singularities on the other blades and key blade control points and other blade induced velocity contributions are correspondingly greatly reduced, Kerwin and Lee use coarser grids on the other blades and on their downstream wake sheets. This segment reduction for other blades and wakes is also used in CAVITY to improve computational efficiency. For the other blades, five bound vortex segments are used in each of three chordwise strips using every second chord station and every third trailer radius of the key blade grid. Other blade wakes have three trailing segments in the near transition wake up to their roll up points and straight line shed and trailing vortex segments for the other blade wakes are defined by joining every fifth trailing segment end point on every third trailer radius of the key blade wake. The effective strengths of the reduced singularities are obtained from appropriate sums of the strengths of original segments covering the same extent of the blade or wake both streamwise and radially. Other blade segment strengths can be obtained as updates of key blade strengths obtained at previous time steps. The same rolled up tip vortex helix and hub vortex models are used for all blades with the tip vortex helices for each blade just rotated by the inter-blade spacing angle.

In CAVITY, this reduction in other blade singularity segments applies only to the vortex and blade thickness source segments which are fixed in the number contributing for all time. Since the number of cavity source segments that are turned on in each chordwise strip varies with both radius and blade angular position and is often zero or just a few segments close to the leading edge, identical cavity source locations are defined on each blade with other blade extents and source strengths updated each revolution from key blade results.

As in the PUF-2 code, CAVITY uses a reduced number of flow tangency control points on the key blade at which to evaluate other blade vortex and thickness source induced velocities. Points corresponding to every second chord and radius station of previously defined flow tangency control points are used. Chordwise and radial interpolations of other blade induced velocity to the full number of control points are then used so that other blade contributions can be added directly to key blade contributions. This procedure also improves the computational efficiency without significantly affecting results. As for cavity source segments, the full number of cavity pressure control points are used on the key blade when evaluating induced velocity contributions from other blade singularities.

4 Solution Procedures

The system of linear equations solved by program CAVITY is a slight modification of the system defined by Lee[2]. The modification concerns the use of equation (3.5) obtained for Van Houten's singularity spacing to eliminate one unknown cavity source strength from the equations that are set up at the control points in a given chordwise strip on a designated key blade. Before defining this modified system, the time-stepping, iterative solution procedures that are used in program CAVITY to solve the equations are described.

The governing equations of Section 2 are satisfied by solving an equivalent system of linear equations for the unknown singularity strengths at each analyzed angular position of the key blade. As with the PUF-2 code, CAVITY evaluates the solution at 60 positions in one revolution at multiples of 6 degrees from the zero degree top vertical position. The problem has a unique back sheet cavitation extent and thickness distribution at each blade position which simultaneously satisfies all boundary conditions imposed for a constant pressure everywhere inside the cavity. The sheet cavity is determined by a trial and error iteration scheme in which the chordwise extent in a single strip or cavitating panel of the vortex grid is adjusted until the Bernoulli equation yields a pressure equal to a specified vapour pressure at all cavity pressure control points within the extent. During the iteration process, the cavity pressure for an assumed extent is then treated as an unknown along with the singularity strengths in a single panel, with the extents and singularity strengths in other panels of the key blade and on other blades being specified by an initial condition or from the latest iteration or update of previous solutions.

The solution for a cavitating propeller is started from the fully-wetted blade solution for vortex and blade thickness source segment strengths with sheet cavitation extents and cavity thickness source strengths set to zero. This is essentially the solution provided for the boundary value problem in the PUF-2 code but modified for the different singularity grid as described in Section 3. Blade thickness source strengths are determined at the outset from the known blade section thickness distributions and are constant in time as the blades rotate. Kelvin's theorems and vortex conservation laws can be used to determine all key blade trailing and shed vortex segment strengths in terms of the instantaneous bound vortex segment strengths on the key blade. Since the vortex strengths and cavitation on the other blades are updated each revolution using previous time step solutions for the key blade, the only unknowns of the problem are the instantaneous cavity chordwise extents, bound vortex strengths and cavity thickness source strengths on the key blade.

To help speed convergence of the solution, the key blade is initially positioned at one of the analyzed angular locations of the fully-wetted solution close to the expected inception position for back sheet cavitation. A small initial cavity extent is then assumed in one chordwise strip

or panel between two adjacent trailing vortex radii and extending a short distance in from the leading edge. The chordwise extent and thickness distributions in each strip represent average values over the radial interval of the strip. Since the midpoints of bound vortex segments are convenient locations on each side of the cavity source segments at which to evaluate cavity thickness using the finite difference relations in Appendix B and because the thickness vanishes at the leading and trailing ends of the cavity in each chordwise strip, at least two bound vortex intervals are required initially to generate a non-vanishing cavity on that strip. Because Van Houten's spacing moves this minimum extent closer to the leading edge, the predictions should be slightly more accurate than Lee's results near the inception and collapse phases of cavity development. More segments or a finer grid of singularities could also be used to further improve results near the leading edge however this would add considerably to the computation time.

Figure 4 illustrates the type of iterations of cavity extent required to generate predictions of back sheet cavitation at a given angular position of the key blade. If chordwise panel m is the current panel being investigated, the cavity extents on other panels of the key blade and on other blades are held fixed while the current extent for panel m is increased or decreased in steps equal to the bound vortex spacings on the blade or shed vortex spacings in the wake until two consecutive extents are found which yield cavity pressures from the Bernoulli equation that straddle the vapour pressure for the cavity. A linear interpolation between the two extents and the two sets of panel singularity strengths obtained as solutions is then performed to yield the extent and singularity strengths corresponding to the required vapour pressure. If the extent becomes less than two elements before the cavity pressure falls below the vapour pressure, then that panel is assumed cavitation free. Having obtained the current solution for panel m, the procedure is repeated for the adjacent chordwise strips moving from the blade root to the tip and back for two or three sweeps until a converged cavity is obtained at the fixed angular position. A faster convergence is obtained after the first panel solution by using the number of cavitating elements for the previous adjacent panel as an initial guess for the current panel.

For second and subsequent blade angular positions or time steps in the first revolution, the solution is again started from the fully-wetted result; however, the initial cavity extents and source strengths for each panel are set equal to those obtained for the same panel at the previous angle or time step and the extents are iterated from there using the local inflow at the new blade position until a new cavity solution converges. As the other blades reach angular positions previously passed by the key blade, the other blade singularity strengths and cavity extents are updated from the latest key blade results at those positions. The procedure continues until two consecutive revolutions have virtually indistinguishable results, which is generally by the end of the third revolution for the cavitating blade. If over the first revolution no back sheet cavitation is predicted, the procedure terminates as a cavitation free operating condition.

The system of linear equations developed by Lee and solved by the preceding iterative method is now described together with the modified forms of the equations used in program CAVITY. Using equations (2.5) and (2.7) for induced velocities from individual source and vortex segments, Lee derives the following set of N linear equations for the flow tangency boundary condition of equation (2.9) applied to a single chordwise panel and fixed angular position of the key blade.

$$\sum_{n=1}^{N} A_{ni}\Gamma_n + \sum_{n=1}^{N_c} B_{ni}Q_n = C_i\,, \quad i = 1,2,...,N \tag{4.1}$$

Although there are N unknown bound vortex strengths Γ_n in each analyzed panel at all angular positions, the number of cavity source segments N_c with strengths Q_n varies both over the blade radius and with blade position. The subscript i refers to the i^{th} flow tangency control point in the analyzed panel. The coefficients A_{ni},B_{ni} and right-hand side C_i in equation (4.1) are obtained from the following relations.

$$A_{ni} = \vec{n}_i \cdot \vec{v}_{ni}^{BVQ} \tag{4.2}$$

$$B_{ni} = \vec{n}_i \cdot \vec{v}_{ni}^{Q} \tag{4.3}$$

$$C_i = -\vec{n}_i \cdot (\vec{V}_{\infty_i} + \vec{V}_i^{SVQ} + \vec{V}_i^{BTS} + \vec{V}_i^{OP} + \vec{V}_i^{OB}) \tag{4.4}$$

In these equations, $\vec{n}_i$ is the unit normal to the mean surface at the i^{th} control point of the selected panel. Velocities $\vec{v}_{ni}^{BVQ}$ and $\vec{v}_{ni}^{Q}$ are induced at the i^{th} control point by the n^{th} unit strength bound vortex quadrilateral and cavity thickness source segment in the analyzed panel. To enforce vorticity conservation, Kerwin and Lee found it convenient to combine the blade vortex segments into closed quadrilateral elements. In a given panel, the n^{th} unit strength bound vortex quadrilateral (BVQ) induces a net velocity equal to the sum of the unit strength contributions from the n^{th} bound vortex segment, the first shed vortex segment, and the outer and inner trailing vortex segments connecting them in the same chordwise strip. In this sum the first shed vortex and inner trailing vortex contributions are of opposite sense to other contributions from the BVQ element. This unit strength BVQ contribution is then multiplied by the current strength of the n^{th} bound vortex segment, Γ_n, to give its total induced velocity at the i^{th} control point.

The right-hand side C_i of equation (4.4) consists of the normal component of all known velocity contributions at the i^{th} control point: $\vec{V}_\infty$, the net relative inflow comprised of steady components opposite to the ship speed and propeller rotation speed and unsteady components due to the ship wake inflow variations; $\vec{V}^{SVQ}$, the velocity induced by all shed vortex quadrilaterals in the key blade's wake; $\vec{V}^{BTS}$, the velocity induced by all key blade thickness sources; $\vec{V}^{OP}$, the induced velocity from all BVQ's and cavity thickness sources in other panels of the key blade; and $\vec{V}^{OB}$, the total induced velocity contribution from other blade singularities. Vorticity conservation laws are again automatically enforced by combining the shed and trailing vortex segments of the near transition wake into closed shed vortex quadrilateral (SVQ) elements. The net induced velocity from the n^{th} unit strength SVQ element consists of the sum of unit strength contributions from the n^{th} and $n+1^{st}$ shed vortex segments in a given panel and the outer and inner trailing vortex segments connecting them. The $n+1^{st}$ shed vortex and inner trailing vortex segment contributions are given the opposite sense to the other contributions from the SVQ element. The strength of an SVQ element is determined from the total circulation around the upstream blade section in the same panel at previous time steps or blade angular positions. The total section circulation at a given time step is the sum of instantaneous

bound vortex segment strengths in the corresponding chordwise strip. At any time step, the unit strength contribution of the first SVQ element in a streamwise panel is multiplied by the section circulation for the previous time step to obtain its total induced velocity contribution at the i^{th} control point. Each time the blade angular position is incremented, the current SVQ strengths are shifted one SVQ element downstream.

Using the wake roll up model described in Section 3, the construction of the last shed vortex elements in each panel is modified to merge smoothly with the rolled up tip and hub vortices in the ultimate wake. The last shed vortex element in the middle streamwise panel is open ended to the end of the ultimate wake. Instead of subtracting a unit strength contribution to induced velocity for a downstream shed vortex segment in the usual closed quadrilateral element, the unit strength tip vortex contribution and the negative of the unit strength hub vortex contribution are added to the last shed and trailing vortex segment contributions in the middle panel. Since all other panels close at either of the two roll up points, the last shed vortex contributions in these panels are from closed triangular elements without the usual contribution from the downstream shed vortex segment. Since the induced velocity contributions from the ultimate wake decrease rapidly with distance downstream and are much smaller than near wake contributions, the precise geometric arrangement and strength distribution of wake vortices near roll up are not as critical to evaluating the solution on the blades as providing a method of properly shedding vorticity into the near wake.

If the cavity extent in a single chordwise panel consists of N_c cavitating elements from the leading edge at a given angular position of the key blade, then Lee defines the following set of N_c linear equations representing equation (2.15) for the cavity dynamics.

$$\sum_{n=1}^{N} D_{ni}\Gamma_n + \sum_{n=1}^{N_c} E_{ni}Q_n - (p - p_\infty) = F_i\,, \quad i = 1, 2, ..., N_c \tag{4.5}$$

The subscript i in equation (4.5) refers to the i^{th} cavity pressure control point in the analyzed panel. The coefficients D_{ni},E_{ni} and right-hand side F_i are obtained from the relations:

$$D_{ni} = \begin{cases} -\frac{\rho}{2\Delta t} - \rho U_i(\vec{s}_i \cdot \vec{v}_{ni}^{BVQ})\,, & n \le i \text{ and } i \le N \\ -\rho U_i(\vec{s}_i \cdot \vec{v}_{ni}^{BVQ})\,, & n > i \text{ or } i > N \end{cases} \tag{4.6}$$

$$E_{ni} = -\frac{\rho}{\Delta t}\phi_{ni}^{Q} - \rho U_i(\vec{s}_i \cdot \vec{v}_{ni}^{Q}) \tag{4.7}$$

$$\begin{aligned} F_i \;=\; & -\sum_{n=1}^{i} \frac{\rho}{2\Delta t}\Gamma_n^{(t-1)} - \sum_{n=1}^{N_c^{(t-1)}} \frac{\rho}{\Delta t}\phi_{ni}^{Q} Q_n^{(t-1)} + \frac{\rho}{\Delta t}(\Phi_i^{OP} - \Phi_i^{OP^{(t-1)}} + \Phi_i^{OB} - \Phi_i^{OB^{(t-1)}}) \\ & + \rho U_i[\vec{s}_i \cdot (\vec{V}_i^{SVQ} + \vec{V}_i^{BTS} + \vec{V}_i^{OP} + \vec{V}_i^{OB})] + \rho g y_{o_i} \end{aligned} \tag{4.8}$$

In the preceding equations, Δt is the time step between analyzed blade positions and $\vec{s}_i$ is a unit vector tangent to the mean surface in the streamwise sense at the i^{th} control point. The

mean relative inflow velocity U in a given chordwise strip is constant for all control points that fall on the blade. For cavities that extend into the wake, U is given a subscript i to account for streamwise variations in the radius of control points in each wake panel due to radial contraction of the trailing vortex sheet. The contribution of vorticity to the induced potential at a control point is obtained as half the sum of bound vortex segment strengths from the leading edge to the i^{th} control point in the analyzed panel. This is the reason for the extra term in D_{ni} when $n \leq i$ and $i \leq N$, and for the first term in F_i. From equation (2.4), ϕ^Q_{ni} is the potential induced at the i^{th} control point by the n^{th} unit strength cavity thickness source segment in the analyzed panel. The superscript $(t-1)$ denotes values of variables at the previous time step arising from the backward time differences used to approximate the potential time derivative in the Bernoulli equation. Potentials Φ^{OP} and Φ^{OB} are induced by all of the cavity thickness sources in other panels of the key blade, and on other blades respectively. Vortex segments in other panels of the key blade, in the downstream wakes, and on other blades, do not contribute to the potential at the i^{th} control point in the analyzed panel. Potential induced by blade thickness sources is constant in time and so does not appear in the time derivative term.

The cavity closure condition derived by Lee for a single panel of the key blade can be written in the form:

$$\sum_{n=1}^{N_c} G_n Q_n = H \tag{4.9}$$

The coefficients G_n and right-hand side H in equation (4.9) are obtained directly from equation (B.3) in Appendix B.

Lee uses equations (4.1), (4.5) and (4.9) together to define a system of $N+N_c+1$ equations for the same number of unknowns: Γ_n , $n = 1, 2, ..., N$; Q_n , $n = 1, 2, ..., N_c$; and $(p-p_\infty)$. When equation (3.5) is used to substitute for Q_1 in terms of Γ_1 in each of these equations, the result is the following set of $N + N_c$ linear equations.

$$(A_{1i} + 4^{3/4} B_{1i})\Gamma_1 + \sum_{n=2}^{N} A_{ni}\Gamma_n + \sum_{n=2}^{N_c} B_{ni} Q_n = C_i\,, \quad i = 1, 2, ..., N \tag{4.10}$$

$$(D_{1i} + 4^{3/4} E_{1i})\Gamma_1 + \sum_{n=2}^{N} D_{ni}\Gamma_n + \sum_{n=2}^{N_c} E_{ni} Q_n - (p - p_\infty) = F_i\,, \quad i = 1, 2, ..., N_c - 1 \tag{4.11}$$

$$4^{3/4} G_1 \Gamma_1 + \sum_{n=2}^{N_c} G_n Q_n = H \tag{4.12}$$

Note that elimination of the first cavity source segment strength from Lee's system allows elimination of the first cavity pressure control point in each panel and gives the control point distribution described in Section 3 for Van Houten's singularity spacing. This also requires that the number of bound vortex segments contributing to the sums for potential at the new i^{th}

cavity pressure control point be increased by one in the modified system. Equations (4.6) and (4.8) for D_{ni} and F_i are then replaced by the following two equations in program CAVITY.

$$D_{ni} = \begin{cases} -\frac{\rho}{2\Delta t} - \rho U_i(\vec{s}_i \cdot \vec{v}_{ni}^{BVQ}), & n \le i+1 \text{ and } i < N \\ -\rho U_i(\vec{s}_i \cdot \vec{v}_{ni}^{BVQ}), & n > i+1 \text{ or } i \ge N \end{cases} \tag{4.13}$$

$$\begin{aligned} F_i = & -\sum_{n=1}^{i+1} \frac{\rho}{2\Delta t}\Gamma_n^{(t-1)} - \sum_{n=1}^{N_c^{(t-1)}} \frac{\rho}{\Delta t}\phi_{ni}^{Q} Q_n^{(t-1)} + \frac{\rho}{\Delta t}(\Phi_i^{OP} - \Phi_i^{OP^{(t-1)}} + \Phi_i^{OB} - \Phi_i^{OB^{(t-1)}}) \\ & + \rho U_i[\vec{s}_i \cdot (\vec{V}_i^{SVQ} + \vec{V}_i^{BTS} + \vec{V}_i^{OP} + \vec{V}_i^{OB})] + \rho g y_{o_i} \end{aligned} \tag{4.14}$$

5 Correlation of Theory and Experiment

In this section chordwise extent predictions for back sheet cavitation obtained with program CAVITY are compared with experimental data for three propeller models tested at the Maritime Research Institute Netherlands (MARIN), formerly the Netherlands Ship Model Basin (NSMB), and for one full scale propeller. All of the propeller models had five blades and operated as twin screw configurations at Froude scaled conditions with advance coefficients and cavitation numbers matching the full scale values. In the model tests, roughness elements were applied to the blade leading edges to trip the blade boundary layers from laminar to turbulent and better approximate the flow conditions both at full scale and in the theory. The full scale propeller had four blades and operated in the large wake deficit region behind a single screw merchant ship. The behind condition advance coefficients, $J = V_s(1 - w_T)/(nD)$, and shaft depth cavitation numbers, $\sigma_n = (p_\infty - p_v)/(\frac{1}{2}\rho n^2 D^2)$, for all of the propellers examined are provided in Table 1. For these dimensionless coefficients, V_s is vessel speed, w_T is the wake fraction defined in section 2, n is rotation speed in revolutions per second, D is propeller diameter, ρ is water density, p_v is the vapour pressure of water and p_∞ is the shaft depth pressure at upstream infinity defined by equation 2.14 of section 2.

Tables 2 through 4 provide the radial distributions of blade geometric parameters for the propeller models. Propeller model 5349 is fixed pitch while models 5268 and 5733 are variable pitch. Pitch and rake to diameter ratios, P/D and x_R/D, skew angle in degrees, θ_s, chord to diameter ratio, c/D, and maximum camber and thickness to chord ratios, f_o/c and t_o/c, are provided versus the blade radius fraction, r/r_T. Models 5349 and 5268 have sections with a NACA 65 mean camber line while model 5733 uses a NACA $a = 0.8$ mean line. Calculations were obtained using the modified NACA 66 section thickness form that is the default form used with the PUF-2 code. Details of the propeller geometry for the merchant ship were provided by Raestad[9] as part of a study organized by NSMB Cooperative Research Ships. Full scale

cavitation extent data for this propeller at three blade angular positions and a single ship speed were also provided by Raestad[10] through the Cooperative Research Ships program.

The circumferential variation of the axial, radial and tangential components of the ship wake inflow velocity divided by ship speed as measured in the propeller rotation plane can be expanded in the following Fourier series in rotation plane angle θ measured in a clockwise sense looking downstream from a top vertical reference position.

$$\frac{V}{V_s} = A_o + \sum_{m=1}^{\infty} [A_m \cos(m\theta) + B_m \sin(m\theta)] \tag{5.1}$$

The ship wake axial component is defined positive downstream, the radial component is positive outward and the tangential component is positive in the positive θ direction, or clockwise looking downstream. The Fourier series coefficients for the measured nominal wake used with propeller model 5349 are given in Tables 5 to 7 while Tables 8 to 10 provide the coefficients of the common nominal wake used for both models 5268 and 5733. BSRA wake scaling methods[4] and VERITEC effective wake corrections[6] were applied to the axial component of the nominal wake distribution for the merchant ship to generate the effective, full scale wake distribution used in the numerical predictions with program CAVITY.

Figures 5 through 7 compare the chordwise extents of back sheet cavitation obtained with program CAVITY with experimental observations for the three model propellers. These figures are projected views of one blade of the propellers looking downstream into the plane of rotation for 6 selected angular positions between -180 and 180 degrees that increase counter-clockwise with 0 degrees at the top vertical position. Predicted extents are represented by the solid line splined through the ends of the dashed chord lines drawn as fixed radius cir ular arcs from the leading edge to the cavity trailing end in the projected blade view. Model test chordwise extents are indicated by the centres of the small circles. A very good correlation is obtained for the unskewed, large aspect ratio blade of propeller 5349 using the three orthogonal components of the measured nominal wake for the predictions. Although not correlating quite as well, the numerical predictions for the more typical low aspect ratio blade of propeller 5268 do show the extents developing beyond the trailing edge at the 60 degree position. The poorest correlation is obtained for propeller 5733 for which CAVITY failed to predict the large extents developing on the lower radius sections of the blade. When the thick root sections of this blade cavitate, poor results might be expected due to violation of the thin section assumption of lifting surface methods.

Figure 8 indicates how well the numerical method can predict full scale sheet cavitation extents for the single propeller merchant ship when a scaled, effective wake, axial velocity component and nominal wake, radial and tangential velocity components are used for the predictions. Considering the uncertainty in the accuracy of the calculated effective ship wake distribution, a good extent correlation is obtained for the three angular positions at which full scale extent data is provided. Similar calculations performed using the three components of the measured nominal wake distribution greatly overestimated the sheet cavitation extents.

6 Concluding Remarks

A computer code CAVITY has been developed at DREA based on MIT lifting surface procedures for predicting the development of back sheet cavitation chordwise extents and thickness distributions on marine propellers operating in a ship's wake. CAVITY uses an improved chord distribution of singularity segments and boundary condition control points over that used in the original MIT procedure and incorporates the PUF-2 model for radial contraction and roll-up of the downstream wake sheets to provide good estimates of the chordwise extents of back sheet cavitation compared with experimental data.

The use of the measured nominal inflow wake seems to provide acceptable extent predictions compared with model test data in twin propeller applications. The one example of full scale extent predictions included for a single screw vessel revealed that Reynolds number scaling and effective wake corrections can significantly improve the numerical results for a propeller operating in a large wake deficit. Large sheet cavitation extents developing on thick root sections of a blade are not predicted well by the lifting surface method. Perhaps a surface panel singularity method that uses cavity source and vorticity distributions over the actual blade surfaces may be required to improve these results.

Sheet cavitation thickness correlations of theory and experiment have not been included in this study due to the difficulty of obtaining reliable experimental data. Future experiments should consider sheet cavity thickness measurements for verification of numerical predictions since thickness distributions and associated cavity source strengths are required to calculate radiated noise levels and propeller induced hull pressures.

Propeller	J	σ_n
Model 5349	1.06	5.38
Model 5268	0.92	1.30
Model 5733	1.03	1.65
Full Scale	0.75	1.96

Table 1: Propeller Operating Conditions

r/r_T	P/D	x_R/D	θ_s [deg.]	c/D	f_o/c	t_o/c
0.2067	0.9625	−0.0043	−3.237	0.1490	0.0257	0.2539
0.2563	1.2210	0.0014	−2.573	0.1490	0.0257	0.2539
0.3058	1.2461	0.0159	−2.710	0.1463	0.0456	0.2386
0.4050	1.3440	0.0372	−2.733	0.1437	0.0679	0.2071
0.5042	1.4343	0.0554	−2.521	0.1487	0.0717	0.1670
0.6033	1.4718	0.0724	−2.189	0.1542	0.0654	0.1270
0.7025	1.4530	0.0882	−1.759	0.1560	0.0524	0.0924
0.8017	1.3720	0.1029	−1.243	0.1495	0.0334	0.0647
0.9008	1.2660	0.1172	−0.659	0.1295	0.0150	0.0490
0.9504	1.2282	0.1243	−0.332	0.1072	0.0062	0.0498
1.0000	1.2090	0.1313	0.000	0.0442	0.0000	0.1132

Table 2: Blade geometry for propeller model 5349

r/r_T	P/D	x_R/D	θ_s[deg.]	c/D	f_o/c	t_o/c
0.3385	1.2684	0.0092	2.613	0.2127	0.0116	0.2101
0.4000	1.2758	0.0086	2.412	0.2506	0.0164	0.1511
0.5000	1.2799	0.0089	2.515	0.3125	0.0174	0.0899
0.6000	1.2727	0.0114	3.209	0.3656	0.0163	0.0560
0.7000	1.2546	0.0150	4.320	0.3958	0.0150	0.0373
0.8000	1.2244	0.0179	5.271	0.3886	0.0139	0.0264
0.8500	1.2048	0.0188	5.604	0.3644	0.0134	0.0229
0.9000	1.1812	0.0190	5.781	0.3193	0.0130	0.0202
0.9500	1.1539	0.0189	5.901	0.2422	0.0121	0.0192
0.9750	1.1385	0.0197	6.240	0.1805	0.0114	0.0211
1.0000	1.1207	0.0186	5.982	0.0000	0.0000	0.0000

Table 3: Blade geometry for propeller model 5268

r/r_T	P/D	x_R/D	θ_s[deg.]	c/D	f_o/c	t_o/c
0.2981	1.0550	0.0087	2.956	0.1900	0.0000	0.2602
0.3500	1.3230	0.0093	−2.412	0.2200	0.0075	0.1974
0.4000	1.4680	0.0100	−5.535	0.2500	0.0123	0.1518
0.5000	1.5780	0.0113	−7.368	0.3130	0.0186	0.0908
0.6000	1.5580	0.0126	−5.397	0.3730	0.0197	0.0552
0.7000	1.4960	0.0140	−1.541	0.4090	0.0187	0.0366
0.8000	1.3940	0.0153	3.438	0.4020	0.0155	0.0261
0.9000	1.2000	0.0166	8.812	0.3310	0.0097	0.0198
0.9500	1.0510	0.0173	11.367	0.2530	0.0054	0.0187
0.9750	0.9580	0.0176	12.611	0.1910	0.0015	0.0202
1.0000	0.8430	0.0179	13.740	0.0000	0.0000	0.0000

Table 4: Blade geometry for propeller model 5733

r/r_T	0.328		0.459		0.591		0.722	
m	A_m	B_m	A_m	B_m	A_m	B_m	A_m	B_m
0	0.9606		0.9535		0.9449		0.9397	
1	−0.0442	−0.0206	−0.0473	−0.0200	−0.0575	−0.0248	−0.0671	−0.0281
2	−0.0269	−0.0230	−0.0288	−0.0269	−0.0356	−0.0348	−0.0394	−0.0394
3	−0.0105	−0.0377	−0.0103	−0.0378	−0.0120	−0.0423	−0.0145	−0.0433
4	−0.0004	−0.0276	0.0006	−0.0263	−0.0003	−0.0277	−0.0013	−0.0266
5	0.0111	−0.0212	0.0107	−0.0227	0.0096	−0.0228	0.0054	−0.0185
6	0.0176	−0.0147	0.0182	−0.0147	0.0167	−0.0167	0.0114	−0.0136
7	0.0204	−0.0043	0.0199	−0.0024	0.0185	−0.0071	0.0135	−0.0059
8	0.0173	0.0037	0.0157	0.0047	0.0167	0.0010	0.0125	−0.0006
9	0.0101	0.0082	0.0089	0.0061	0.0114	0.0051	0.0087	0.0034
10	0.0065	0.0100	0.0060	0.0079	0.0073	0.0080	0.0066	0.0066
11	0.0011	0.0091	0.0002	0.0089	0.0019	0.0089	0.0025	0.0083
12	−0.0022	0.0062	−0.0039	0.0065	−0.0013	0.0073	−0.0005	0.0074
13	−0.0036	0.0029	−0.0047	0.0028	−0.0027	0.0047	−0.0025	0.0050
14	−0.0032	0.0003	−0.0035	0.0006	−0.0026	0.0028	−0.0028	0.0030
15	−0.0025	−0.0012	−0.0025	−0.0006	−0.0026	0.0012	−0.0029	0.0015

r/r_T	0.853		0.919		0.984		1.050	
m	A_m	B_m	A_m	B_m	A_m	B_m	A_m	B_m
0	0.9272		0.9176		0.9071		0.9092	
1	−0.0825	−0.0345	−0.0950	−0.0423	−0.1065	−0.0494	−0.1103	−0.0533
2	−0.0460	−0.0501	−0.0506	−0.0580	−0.0571	−0.0673	−0.0548	−0.0690
3	−0.0153	−0.0474	−0.0133	−0.0531	−0.0146	−0.0585	−0.0132	−0.0622
4	−0.0014	−0.0241	−0.0004	−0.0253	0.0033	−0.0244	0.0045	−0.0257
5	0.0022	−0.0142	0.0010	−0.0119	0.0011	−0.0090	0.0020	−0.0097
6	0.0029	−0.0129	0.0015	−0.0099	−0.0010	−0.0063	−0.0001	−0.0064
7	0.0085	−0.0069	0.0032	−0.0078	−0.0001	−0.0048	0.0023	−0.0057
8	0.0086	−0.0018	0.0056	−0.0070	0.0015	−0.0047	0.0014	−0.0053
9	0.0072	0.0009	0.0083	−0.0030	0.0040	−0.0042	0.0047	−0.0042
10	0.0063	0.0043	0.0084	0.0030	0.0059	−0.0009	0.0062	0.0000
11	0.0032	0.0072	0.0051	0.0070	0.0053	0.0031	0.0062	0.0041
12	−0.0002	0.0066	0.0015	0.0066	0.0033	0.0045	0.0028	0.0050
13	−0.0014	0.0046	−0.0004	0.0045	0.0016	0.0046	0.0009	0.0040
14	−0.0027	0.0031	−0.0015	0.0033	−0.0007	0.0046	−0.0015	0.0032
15	−0.0032	0.0014	−0.0023	0.0025	−0.0028	0.0034	−0.0026	0.0022

Table 5: Axial Component of Nominal Wake for Propeller Model 5349

r/r_T	0.328		0.459		0.591		0.722	
m	A_m	B_m	A_m	B_m	A_m	B_m	A_m	B_m
0	0.0513		0.0277		0.0167		0.0098	
1	0.1085	0.0529	0.1234	0.0610	0.1251	0.0599	0.1281	0.0608
2	−0.0113	−0.0011	−0.0029	0.0087	0.0002	0.0122	0.0040	0.0157
3	−0.0087	−0.0182	−0.0044	−0.0088	−0.0057	−0.0085	−0.0045	−0.0073
4	−0.0010	−0.0161	−0.0009	−0.0091	−0.0003	−0.0094	0.0001	−0.0087
5	0.0045	−0.0125	0.0029	−0.0081	0.0034	−0.0074	0.0026	−0.0068
6	0.0062	−0.0078	0.0038	−0.0049	0.0042	−0.0057	0.0033	−0.0051
7	0.0074	−0.0046	0.0055	−0.0032	0.0059	−0.0036	0.0045	−0.0040
8	0.0073	−0.0004	0.0057	0.0000	0.0059	−0.0004	0.0053	−0.0011
9	0.0053	0.0015	0.0036	0.0012	0.0047	0.0012	0.0042	0.0005
10	0.0037	0.0027	0.0024	0.0022	0.0035	0.0022	0.0034	0.0021
11	0.0016	0.0030	0.0004	0.0025	0.0017	0.0027	0.0016	0.0030
12	0.0001	0.0025	−0.0006	0.0018	0.0003	0.0025	0.0002	0.0029
13	−0.0008	0.0017	−0.0009	0.0010	−0.0003	0.0020	−0.0008	0.0022
14	−0.0010	0.0011	−0.0008	0.0049	−0.0006	0.0016	−0.0011	0.0015
15	−0.0010	0.0003	−0.0007	−0.0002	−0.0008	0.0009	−0.0012	0.0007

r/r_T	0.853		0.919		0.984		1.050	
m	A_m	B_m	A_m	B_m	A_m	B_m	A_m	B_m
0	0.0079		0.0053		0.0015		0.0018	
1	0.1296	0.0602	0.1294	0.0601	0.1282	0.0582	0.1271	0.0574
2	0.0068	0.0186	0.0068	0.0208	0.0072	0.0206	0.0068	0.0201
3	−0.0037	−0.0057	−0.0038	−0.0054	−0.0039	−0.0067	−0.0041	−0.0071
4	0.0004	−0.0081	0.0004	−0.0072	0.0008	−0.0079	0.0011	−0.0090
5	0.0029	−0.0052	0.0016	−0.0040	0.0020	−0.0036	0.0028	−0.0046
6	0.0019	−0.0038	−0.0001	−0.0031	0.0000	−0.0018	0.0009	−0.0023
7	0.0026	−0.0036	0.0005	−0.0041	−0.0001	−0.0030	0.0005	−0.0037
8	0.0034	−0.0016	0.0018	−0.0027	0.0006	−0.0022	0.0011	−0.0028
9	0.0029	0.0002	0.0021	−0.0016	0.0007	−0.0018	0.0013	−0.0019
10	0.0024	0.0017	0.0025	0.0001	0.0017	−0.0004	0.0020	−0.0004
11	0.0009	0.0024	0.0015	0.0015	0.0013	0.0009	0.0018	0.0009
12	−0.0002	0.0022	0.0005	0.0018	0.0007	0.0014	0.0011	0.0017
13	−0.0008	0.0016	0.0011	0.0012	0.0000	0.0014	0.0000	0.0019
14	−0.0009	0.0011	−0.0004	0.0011	−0.0004	0.0012	−0.0007	0.0014
15	−0.0009	0.0006	−0.0006	0.0007	−0.0007	0.0006	−0.0010	0.0007

Table 6: Radial Component of Nominal Wake for Propeller Model 5349

r/r_T	0.328		0.459		0.591		0.722	
m	A_m	B_m	A_m	B_m	A_m	B_m	A_m	B_m
0	0.0535		0.0464		0.0393		0.0388	
1	0.0630	−0.1383	0.0739	−0.1783	0.0755	−0.1712	0.0705	−0.1686
2	0.0290	−0.0176	0.0217	−0.0200	0.0285	−0.0167	0.0312	−0.0178
3	0.0206	−0.0054	0.0115	−0.0104	0.0122	−0.0053	0.0129	−0.0049
4	0.0166	0.0034	0.0103	−0.0048	0.0100	−0.0002	0.0089	−0.0006
5	0.0110	0.0084	0.0091	−0.0011	0.0067	0.0042	0.0052	0.0032
6	0.0064	0.0098	0.0088	0.0011	0.0044	0.0056	0.0035	0.0050
7	0.0017	0.0119	0.0065	0.0044	0.0008	0.0075	0.0007	0.0066
8	−0.0028	0.0102	0.0042	0.0055	−0.0015	0.0067	−0.0024	0.0056
9	−0.0062	0.0077	0.0010	0.0067	−0.0040	0.0057	−0.0045	0.0048
10	−0.0082	0.0039	−0.0016	0.0059	−0.0060	0.0030	−0.0060	0.0026
11	−0.0084	0.0001	−0.0032	0.0040	−0.0062	0.0001	−0.0059	−0.0001
12	−0.0071	−0.0030	−0.0034	0.0023	−0.0050	−0.0020	−0.0049	−0.0022
13	−0.0046	−0.0049	−0.0032	0.0008	−0.0037	−0.0034	−0.0031	−0.0034
14	−0.0016	−0.0055	−0.0022	−0.0004	−0.0014	−0.0038	−0.0010	−0.0039
15	0.0009	−0.0045	−0.0013	−0.0008	0.0006	−0.0040	0.0009	−0.0035

r/r_T	0.853		0.919		0.984		1.050	
m	A_m	B_m	A_m	B_m	A_m	B_m	A_m	B_m
0	0.0367		0.0339		0.0325		0.0320	
1	0.0676	−0.1665	0.0067	−0.0165	0.0672	−0.1639	0.0667	−0.1626
2	0.0321	−0.0187	0.0805	−0.0424	0.0369	−0.0177	0.0359	−0.0177
3	0.0104	−0.0035	0.0098	−0.0033	0.0083	−0.0010	0.0084	−0.0005
4	0.0064	−0.0015	0.0050	−0.0026	0.0022	−0.0016	0.0027	−0.0027
5	0.0039	0.0013	0.0027	−0.0004	0.0014	−0.0024	0.0015	−0.0022
6	0.0030	0.0029	0.0035	0.0012	0.0040	−0.0014	0.0031	−0.0015
7	0.0007	0.0063	0.0018	0.0060	0.0024	0.0046	0.0015	0.0038
8	−0.0019	0.0053	−0.0013	0.0058	−0.0012	0.0055	−0.0009	0.0050
9	−0.0041	0.0041	−0.0038	0.0046	−0.0030	0.0052	−0.0028	0.0051
10	−0.0059	0.0017	−0.0061	0.0020	−0.0049	0.0027	−0.0050	0.0026
11	−0.0055	−0.0002	−0.0058	−0.0002	−0.0050	0.0000	−0.0052	0.0000
12	−0.0040	−0.0018	−0.0043	−0.0021	−0.0044	−0.0020	−0.0045	−0.0018
13	−0.0025	−0.0030	−0.0023	−0.0033	−0.0024	−0.0028	−0.0029	−0.0028
14	−0.0009	−0.0037	−0.0008	−0.0037	−0.0005	−0.0030	−0.0009	−0.0034
15	0.0007	−0.0033	0.0007	−0.0032	0.0010	−0.0025	0.0011	−0.0030

Table 7: Tangential Component of Nominal Wake for Propeller Model 5349

r/r_T	0.362 (0.349)*		0.481 (464)		0.602 (0.581)		0.723 (0.698)	
m	A_m	B_m	A_m	B_m	A_m	B_m	A_m	B_m
0	0.9788		0.9817		0.9702		0.9670	
1	−0.0616	0.0082	−0.0400	0.0033	−0.0463	0.0029	−0.0527	0.0126
2	−0.0388	0.0303	−0.0351	0.0136	−0.0437	0.0119	−0.0441	0.0165
3	−0.0364	0.0311	−0.0327	0.0157	−0.0312	0.0123	−0.0260	0.0175
4	−0.0238	0.0267	−0.0131	0.0158	-0.0056	0.0130	−0.0015	0.0087
5	−0.0115	0.0198	−0.0029	0.0132	0.0012	0.0088	0.0039	0.0030

r/r_T	0.843 (0.813)		0.964 (0.930)	
m	A_m	B_m	A_m	B_m
0	0.9570		0.9505	
1	−0.0573	0.0103	−0.0753	0.0102
2	−0.0470	0.0157	−0.0614	0.0123
3	−0.0304	0.0108	−0.0374	0.0068
4	−0.0088	0.0036	−0.0107	−0.0040
5	−0.0066	0.0023	−0.0073	−0.0023

Table 8: Axial Component of Nominal Wake for Propeller Models 5268 and 5733
* Note: Radius fractions for Model 5733 in parenthesis

r/r_T	0.362 (0.349)*		0.481 (464)		0.602 (0.581)		0.723 (0.698)	
m	A_m	B_m	A_m	B_m	A_m	B_m	A_m	B_m
0	−0.0930		−0.0491		−0.0223		−0.0088	
1	0.0960	0.0131	0.1134	0.0031	0.1294	−0.0029	0.1338	−0.0107
2	0.0005	0.0119	0.0038	0.0075	0.0077	0.0010	0.0075	−0.0001
3	−0.0109	0.0149	−0.0099	0.0119	−0.0092	0.0052	−0.0072	0.0050
4	−0.0061	0.0127	−0.0070	0.0109	−0.0077	0.0049	−0.0065	0.0052
5	−0.0020	0.0103	−0.0039	0.0094	−0.0047	0.0050	−0.0026	0.0035

r/r_T	0.843 (0.813)		0.964 (0.930)	
m	A_m	B_m	A_m	B_m
0	0.0007		0.0063	
1	0.1395	−0.0180	0.1394	−0.0179
2	0.0090	−0.0048	0.0108	−0.0049
3	−0.0065	0.0013	−0.0053	0.0018
4	−0.0055	0.0038	−0.0054	0.0027
5	−0.0036	0.0028	−0.0036	0.0014

Table 9: Radial Component of Nominal Wake for Propeller Models 5268 and 5733
* Note: Radius fractions for Model 5733 in parenthesis

r/r_T	0.362 (0.349)*		0.481 (464)		0.602 (0.581)		0.723 (0.698)	
m	A_m	B_m	A_m	B_m	A_m	B_m	A_m	B_m
0	−0.0231		−0.0203		−0.0153		−0.0114	
1	−0.0238	−0.1941	−0.0309	−0.1784	−0.0287	−0.1650	−0.0249	−0.1580
2	−0.0018	−0.0101	−0.0038	−0.0125	−0.0061	−0.0117	−0.0025	−0.0094
3	−0.0018	−0.0017	−0.0088	−0.0056	−0.0090	−0.0042	−0.0051	0.0001
4	−0.0049	−0.0107	−0.0047	−0.0052	−0.0044	−0.0016	−0.0013	0.0024
5	−0.0042	0.0048	−0.0035	−0.0013	−0.0048	0.0003	−0.0017	0.0036

r/r_T	0.843 (0.813)		0.964 (0.930)	
m	A_m	B_m	A_m	B_m
0	−0.0056		−0.0042	
1	−0.0209	−0.1591	−0.0164	−0.1533
2	0.0006	−0.0136	0.0036	−0.0146
3	−0.0035	−0.0032	−0.0011	−0.0047
4	−0.0002	0.0011	0.0025	−0.0013
5	−0.0021	0.0032	0.0007	0.0024

Table 10: Tangential Component of Nominal Wake for Propeller Models 5268 and 5733
* Note: Radius fractions for Model 5733 in parenthesis

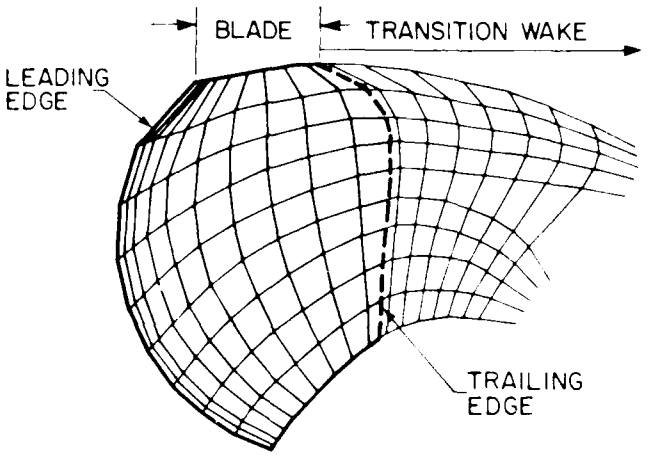

Figure 1a: Blade and Near Wake

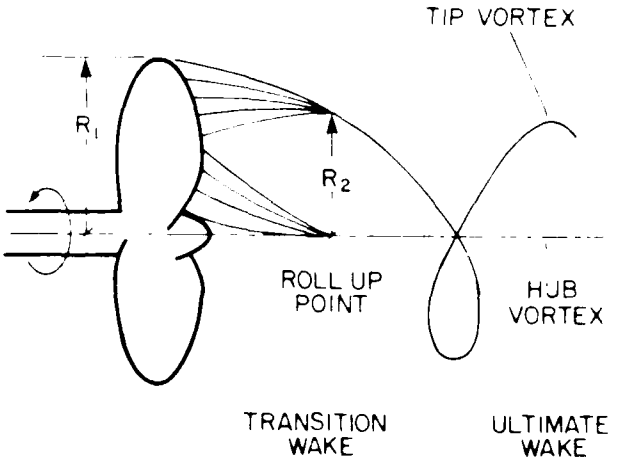

Figure 1b: Roll Up and Ultimate Wake

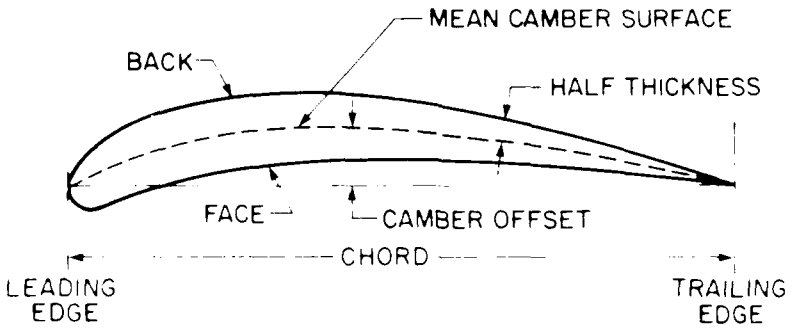

Figure 2a: Blade Section Geometry

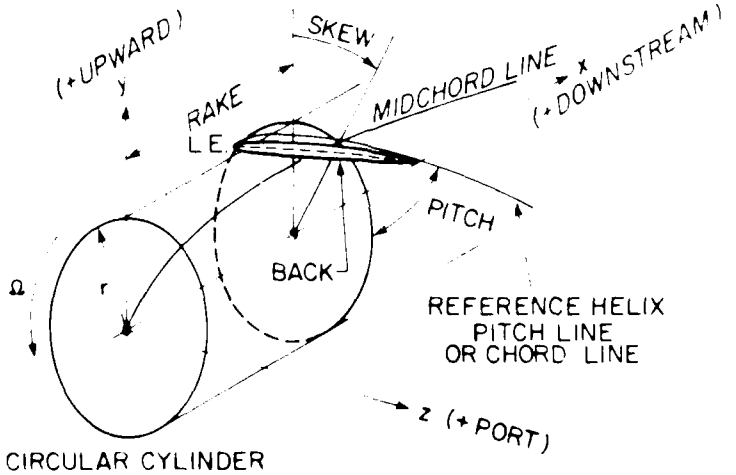

Figure 2b: Propeller Blade Geometry

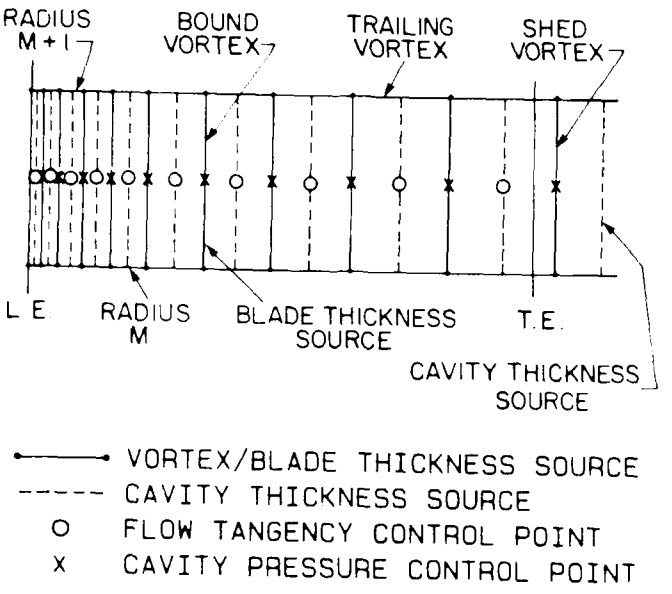

Figure 3: Relative Positioning of Vortices, Sources and Control Points

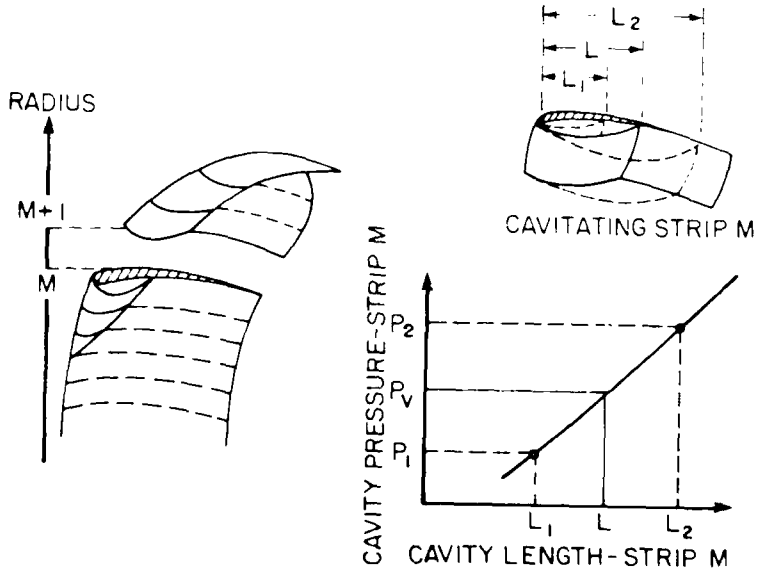

Figure 4: Iterative Solution for Sheet Cavity Extents

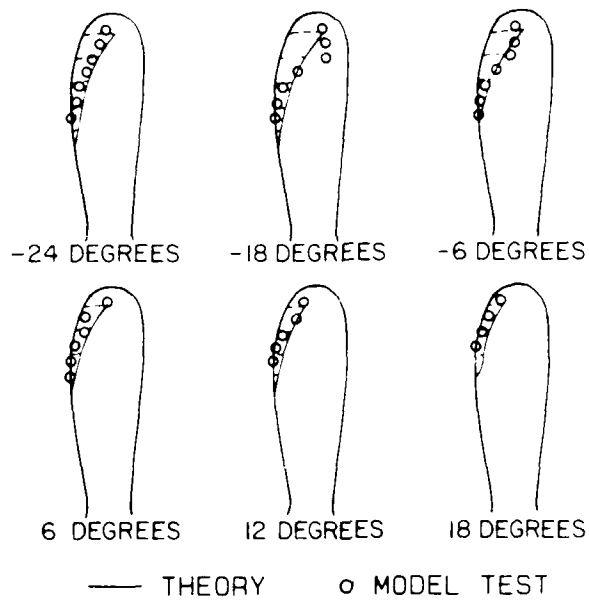

Figure 5: Cavitation Extent Correlation - Model 5349

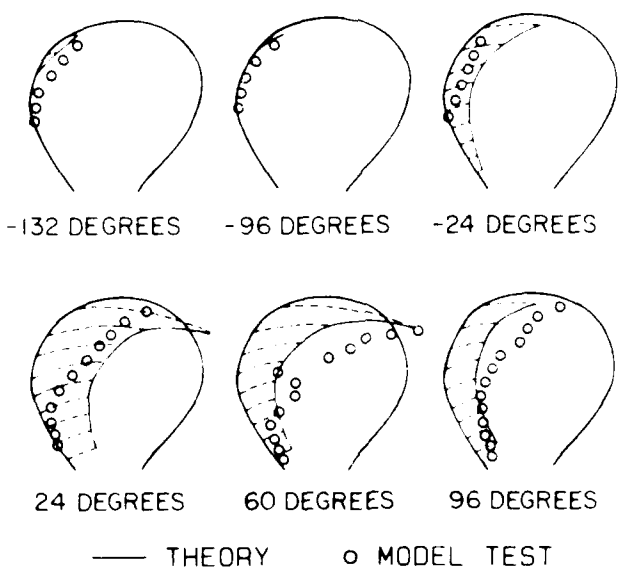

Figure 6: Cavitation Extent Correlation - Model 5268

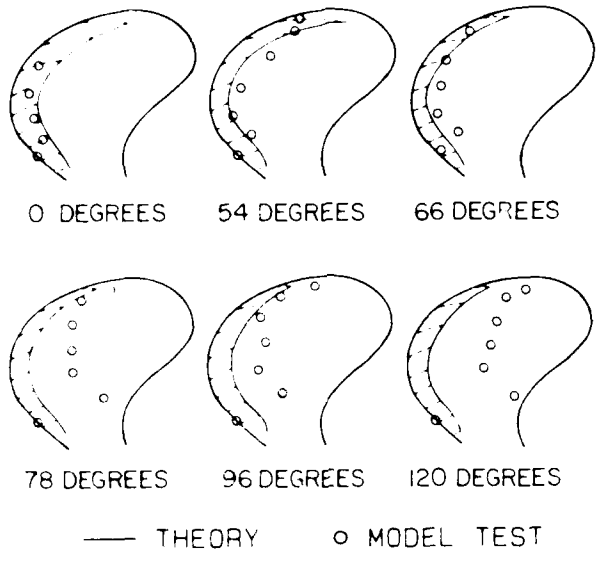

Figure 7: Cavitation Extent Correlation - Model 5733

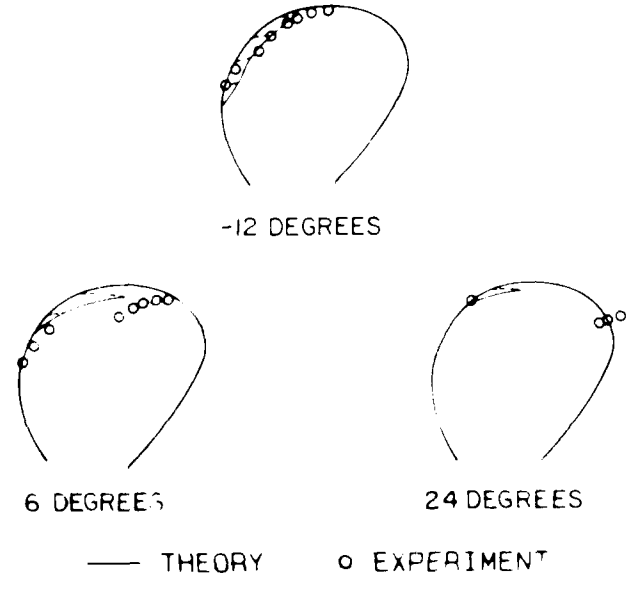

Figure 8: Cavitation Extent Correlation - Full Scale Merchant Ship

Appendix A Potential and Velocity Induced by Straight Line Singularity Segments of Unit Strength

The potential ϕ^Q and velocity $\vec{v}^Q$ induced at point $P = (x, y, z)$ by a straight line source segment of unit strength extending from $P_1 = (x_1, y_1, z_1)$ to $P_2 = (x_2, y_2, z_2)$ are obtained from the following relations.

$$\phi^Q = \begin{cases} -\frac{1}{4\pi} \ln \left| \frac{a-e+b}{c-e} \right|, & c \neq e \\ -\frac{1}{4\pi} \ln \left| \frac{a-e}{e} \right|, & c = e \end{cases} \tag{A.1}$$

where

$$a = \sqrt{(x_2 - x_1)^2 + (y_2 - y_1)^2 + (z_2 - z_1)^2}$$

$$b = \sqrt{(x - x_2)^2 + (y - y_2)^2 + (z - z_2)^2}$$

$$c = \sqrt{(x - x_1)^2 + (y - y_1)^2 + (z - z_1)^2}$$

$$d = \sqrt{c^2 - e^2}, \qquad e = \frac{a^2 + c^2 - b^2}{2a}$$

$$\vec{v}^Q = v_1 \vec{e}_1 + v_2 \vec{e}_2 \tag{A.2}$$

where

$$v_1 = \frac{1}{4\pi}\left(\frac{1}{b} - \frac{1}{c}\right)$$

$$v_2 = \begin{cases} 0, & e = a/2, d = 0 \ (P \text{ at segment midpoint}) \\ -\frac{d}{8\pi}\left[\frac{1}{e^2} - \frac{1}{(a-e)^2}\right], & e < 0, d < 0.03|e| \\ \frac{d}{8\pi}\left[\frac{1}{e^2} - \frac{1}{(a-e)^2}\right], & e > a, d < 0.03|e| \\ -\frac{1}{4\pi d}\left(\frac{e}{c} + \frac{a-e}{b}\right), & \text{otherwise} \end{cases}$$

$$\vec{e}_1 = \frac{1}{a}(x_2 - x_1\,,\, y_2 - y_1\,,\, z_2 - z_1)$$

$$\vec{e}_2 = \frac{1}{d}(x_e - x\,,\, y_e - y\,,\, z_e - z)$$

$$x_e = x_1 + \frac{e}{a}(x_2 - x_1)\,, \qquad y_e = y_1 + \frac{e}{a}(y_2 - y_1)\,, \qquad z_e = z_1 + \frac{e}{a}(z_2 - z_1)$$

The velocity $\vec{v}^{\Gamma}$ induced at P by a straight line vortex segment of unit strength from P_1 to P_2 is defined as:

$$\vec{v}^{\Gamma} = -\frac{v_2}{ad}(\vec{a} \times \vec{d}) \tag{A.3}$$

where

$$\vec{a} = (x_2 - x_1\,,\, y_2 - y_1\,,\, z_2 - z_1)$$

$$\vec{d} = (x - x_e\,,\, y - y_e\,,\, z - z_e)$$

Variables v_2, a, d, and (x_e, y_e, z_e) are defined in equations (A.1) and (A.2).

Appendix B Relations for Cavity Thickness and Closure

The following discretized version of equation (2.17) relates the thicknesses h_{n-1} and h_n of the sheet cavity at the end points of the chordwise camber surface interval $\Delta\xi_n = \xi_n - \xi_{n-1}$ and over a time interval Δt to the cavity line source segment strengths, Q_n

$$Q_n = \Delta\xi_n \cos\epsilon_n \left(\frac{\bar{h}_n - \bar{h}_n^{(t-1)}}{\Delta t} + U_n \frac{h_n - h_{n-1}}{\Delta\xi_n} \right) \tag{B.1}$$

where

$$\bar{h}_n = \frac{h_n + h_{n-1}}{2}$$

Here, U_n is the mean relative inflow velocity at the n^{th} source segment in a given panel and superscript $(t-1)$ refers to values of h at the previous time step. The leading edge of the blade in each chordwise strip corresponds to $\xi_0 = 0$. This finite difference formula is rearranged by Lee[2] to obtain the following recurrence formula for cavity thickness.

$$h_0 = h_{N_c} = 0$$

$$h_n = \frac{1}{1+R_n} \left[(1-R_n) h_{n-1} + \frac{Q_n}{U_n \cos\epsilon_n} + F R_n \left(h_n^{(t-1)} - h_{n-1}^{(t-1)} \right) \right], \qquad n = 1, 2, \ldots, N_c - 1 \tag{B.2}$$

where

$$R_n = \frac{\Delta\xi_n}{2U_n \Delta t}, \qquad F = \begin{cases} \frac{L^{(t-1)} - \xi_{n-1}}{\Delta\xi_n}, & \xi_{n-1} < L^{(t-1)} < \xi_n \\ 0, & L^{(t-1)} \le \xi_{n-1} \\ 1, & L^{(t-1)} \ge \xi_n \end{cases}$$

Here, $L^{(t-1)}$ is the cavity extent in the given chordwise strip at the previous time step. The values of h_0 and h_{N_c} are set to zero at the leading edge, $\xi = 0$, and cavity trailing end, $\xi = L$, at all time steps.

Lee[2] derives the following numerical cavity closure condition by repetitive use of the preceding recurrence formula.

$$\sum_{n=1}^{N_c-1}\Big(\prod_{k=n+1}^{N_c}\frac{1-R_k}{1+R_k}\Big)\frac{1}{(1+R_n)U_n\cos\epsilon_n}Q_n+\frac{1}{(1+R_{N_c})U_{N_c}\cos\epsilon_{N_c}}Q_{N_c}=\begin{cases}H_1, & N_c^{(t-1)}<N_c\\ H_2, & N_c^{(t-1)}=N_c\\ H_3, & N_c^{(t-1)}>N_c\end{cases} \tag{B.3}$$

where

$$H_1=-\sum_{n=1}^{N_c^{(t-1)}}\Big(\prod_{k=n+1}^{N_c}\frac{1-R_k}{1+R_k}\Big)\frac{F_nR_n}{1+R_n}[h_n^{(t-1)}+h_{n-1}^{(t-1)}]$$

$$F_n=\begin{cases}1, & n<N_c^{(t-1)}\\ \dfrac{L^{(t-1)}-\xi_{(N_c^{(t-1)}-1)}}{\Delta\xi_{N_c^{(t-1)}}}, & n=N_c^{(t-1)}\end{cases}$$

$$H_2=-\sum_{n=1}^{N_c-1}\Big(\prod_{k=n+1}^{N_c}\frac{1-R_k}{1+R_k}\Big)\frac{R_n}{1+R_n}[h_n^{(t-1)}+h_{n-1}^{(t-1)}]-\frac{FR_{N_c}}{1+R_{N_c}}h_{N_c-1}^{(t-1)}$$

$$F=\frac{L^{(t-1)}-\xi_{N_c-1}}{\Delta\xi_{N_c}}$$

$$H_3=-\sum_{n=1}^{N_c-1}\Big(\prod_{k=n+1}^{N_c}\frac{1-R_k}{1+R_k}\Big)\frac{R_n}{1+R_n}[h_n^{(t-1)}+h_{n-1}^{(t-1)}]-\frac{R_{N_c}}{1+R_{N_c}}[h_{N_c}^{(t-1)}+h_{N_c-1}^{(t-1)}]$$

References

1. Kuiper, G., "Physical Aspects of Cavitation Induced Hull-Pressure Fluctuations", NSMB Report No. 45139-1-SR, Jan. 1984. *

2. Lee, C.S., "Prediction of Transient Cavitation on Marine Propellers by Numerical Lifting-Surface Theory", Thirteenth Symposium on Naval Hydrodynamics, Tokyo, Japan, Oct. 1980.

3. Kerwin, J.E. and Lee, C.S., "Prediction of Steady and Unsteady Marine Propeller Performance by Numerical Lifting-Surface Theory", SNAME Transactions, Vol. 86, 1978, pp 218-253.

4. Odabasi, A.Y., "A Pilot Study on the Scale Effect in Near Wakes of Ships", BSRA Contract Report No. W929, Nov. 1982. *

5. Huang, T.T. and Groves, N.C., "Effective Wake: Theory and Experiment", Thirteenth Symposium on Naval Hydrodynamics, Tokyo, Japan, Oct. 1980.

6. Bujnicki, A., "Calculation of Effective Wake by Means of the Method of V-shaped Segments", VERITEC Report No. 83-0293, 1983. *

7. Milne-Thomson, L.M., Theoretical Hydrodynamics, Macmillan Press Ltd., 1968.

8. Van Houten, R.J., "The Numerical Prediction of Unsteady Sheet Cavitation on High Aspect Ratio Hydrofoils", Fourteenth Symposium on Naval Hydrodynamics, Ann Arbor, Michigan, Aug. 1982.

9. Raestad, A.E., "NSMB-Cooperative Research Ships Cavitation Working Group Datasheets", VERITEC Report No. 84-3252, May 1984. *

10. Raestad, A.E., "NSMB-Cooperative Research Ships Cavitation Working Group Task 5, Comparative Predictions of Propeller Induced Hull Pressures, Scaled Wake Distribution", VERITEC Report No. 85-3398, June 1985. *

* References 1, 4, 6, 9 and 10 were produced under contract to the Netherlands Ship Model Basin Cooperative Research Ships organization. Distribution of these reports is limited to Cooperative Research Ships members.

DOCUMENT CONTROL DATA

(Security classification of title, body of abstract and indexing annotation must be entered when the overall document is classified)

1. ORIGINATOR (the name and address of the organization preparing the document. Organizations for whom the document was prepared, e.g. Establishment sponsoring a contractor's report, or tasking agency, are entered in section 12.)

Defence Research Establishment Atlantic

2. DOCUMENT SECURITY CLASSIFICATION (overall security classification of the document including special warning terms if applicable)

Unclassified

3. DOCUMENT TITLE (the complete document title as indicated on the title page. Its classification should be indicated by the appropriate abbreviation (S,C,R or U) in parentheses after the title.)

NUMERICAL PREDICTION OF UNSTEADY SHEET CAVITATION ON MARINE PROPELLERS

4. DESCRIPTIVE NOTES (the category of the document, e.g. technical report, technical note or memorandum. If appropriate, enter the type of report, e.g. interim, progress, summary, annual or final. Give the inclusive dates when a specific reporting period is covered.)

Technical Memorandum

5. AUTHOR(S) (Last name, first name, middle initial. If military, show rank, e.g. Doe, Maj. John E.)

Noble, D.J.

6. DOCUMENT DATE (month and year of publication of document)	7a. NO. OF PAGES (total containing information. Include Annexes, Appendices, etc.)	7b. NO. OF REFS (total cited in document)
JULY 1987	44	10

8a. PROJECT OR GRANT NO. (if appropriate, the applicable research and development project or grant number under which the document was written. Please specify whether project or grant)	8b. CONTRACT NO. (if appropriate, the applicable number under which the document was written)

9a. ORIGINATOR'S DOCUMENT NUMBER (the official document number by which the document is identified by the originating activity. This number must be unique to this document.)	9b. OTHER DOCUMENT NO.(S) (Any other numbers which may be assigned this document either by the originator or by the sponsor.)
DREA TECHNICAL MEMORANDUM 87/203	

10. DOCUMENT AVAILABILITY (any limitations on further dissemination of the document, other than those imposed by security classification)

- (X) Unlimited distribution
- ( ) Distribution limited to defence departments and defence contractors; further distribution only as approved
- ( ) Distribution limited to defence departments and Canadian defence contractors; further distribution only as approved
- ( ) Distribution limited to government departments and agencies; further distribution only as approved
- ( ) Distribution limited to defence departments; further distribution only as approved
- ( ) Other

11. ANNOUNCEMENT AVAILABILITY (any limitation to the bibliographic announcement of this document. This will normally correspond to the Document Availability (10). However, where further distribution (beyond the audience specified in 10) is possible, a wider announcement audience may be selected.)

12. SPONSORING ACTIVITY (the name of the department project office or laboratory sponsoring the research and development. Include the address.)

Defence Research Establishment Atlantic

Unclassified

SECURITY CLASSIFICATION OF FORM

13 ABSTRACT (A brief and factual summary of the document. It may also appear elsewhere in the body of the document itself. It is highly desirable that the abstract of classified documents be unclassified. Each paragraph of the abstract shall begin with an indication of the security classification of the information in the paragraph (unless the document itself is unclassified) represented as (S), (C), or (U). It is not necessary to include here abstracts in both official languages unless the text is bilingual.)

This document describes the theory and numerical methods used in the unsteady analysis program CAVITY that has been developed at the Defence Research Establishment Atlantic (DREA) for the prediction of periodic back sheet cavitation on marine propellers operating in a ship's wake. Sheet cavitation chordwise extent and thickness distributions can be predicted at up to 60 blade angular positions per revolution for a given propeller geometry, operating condition and ship wake input in the propeller rotation plane. The procedures used in CAVITY are based on lifting surface methods developed at the Massachusetts Institute of Technology (MIT) as an extension of the PUF-2 code for predicting both steady and unsteady propeller performance characteristics of marine propellers. The original MIT procedures for the prediction of back sheet cavitation are reviewed and some modifications concerning chordwise distributions of singularities and propeller wake modelling are described. These changes are incorporated to improve predictions of leading edge cavitation development as well as results obtained at off-design operating conditions. Numerical extents obtained with CAVITY are compared to available experimental data. Provided that representative ship wake data are used, the predictions to date for back sheet cavitation show good agreement with experimentally observed extents developing on thin blade sections.

14 KEY WORDS, DESCRIPTORS or IDENTIFIERS (Technically meaningful terms or short phrases that characterize a document and could be helpful in cataloguing the document. They should be selected so that no security classification is required. Identifiers, such as equipment model designation, trade name, military project code name, geographic location may also be included. If possible, keywords should be selected from a published thesaurus, e.g. Thesaurus of Engineering and Scientific Terms (TEST) and that thesaurus identified. If it is not possible to select indexing terms which are Unclassified, the classification of each should be indicated as with the title.)

Sheet Cavitation
Numerical Methods
Marine Propellers
Unsteady Flow
Lifting Surface

Unclassified

SECURITY CLASSIFICATION OF FORM

SAMPLE PRINT OF FORM DCD03A


DATE
FILMED
28